CONSERVATION SCIENCE PARTNERS

FINAL REPORT
JANUARY 6, 2023

Modeling multispecies connectivity across the California Desert Conservation Area, Phase II: Updates to habitat suitability models, resistance surfaces, and management scenarios

Submitted to:

The Bureau of Land Management

PR number: 0040453315
Solicitation number: 140L0619Q0096

Recommended citation: Conservation Science Partners, Inc. 2023. Modeling multispecies connectivity across the California Desert Conservation Area, Phase II: Updates to habitat suitability models, resistance surfaces, and management scenarios. Final Report. Truckee, CA.

CALIFORNIA HEADQUARTERS
11050 PIONEER TRAIL • SUITE 202
TRUCKEE, CALIFORNIA • 96161
(P) 530.214.8905 • (F) 530.214.8907

FORT COLLINS • SEATTLE • FLAGSTAFF
SANTA FE • D.C.
INFO@CSP-INC.ORG
WWW.CSP-INC.ORG

Table of Contents

1. INTRODUCTION

Habitat fragmentation and loss represent primary drivers of species declines (Pimm and Raven 2000, Haddad et al. 2015), and maintaining or restoring linkages between populations of sensitive species in fragmented landscapes is therefore a key conservation goal (Chetkiewicz et al. 2006). Characterizing potential connectivity across a landscape based on species habitat preferences and movement capacity is a critical first step towards this goal, helping to identify areas that will support long-distance movements (e.g., dispersal), promote gene flow among populations (Rayfield et al. 2011, Fletcher et al. 2016), and maintain contiguous movement habitat for species with limited dispersal ability. Ideally, such understanding can be integrated into land use planning to promote the persistence of sensitive wildlife species in multiple-use landscapes (Suraci et al. 2020).

The Mojave Desert ecoregion, including the California Desert Conservation Area (CDCA, Fig. 1), consists largely of public lands, and thus has a multiple-use mandate for most of the landscape. As such, human land uses such as utility-scale renewable energy development (Lovich and Ennen 2011), military operations, and recreation must be balanced with conservation of plants and animals. While some areas of high-quality wildlife habitat have already been lost (Cameron et al. 2012, Gibson et al. 2017), maintaining connections between existing habitat cores for sensitive species is critical to conserving biodiversity in the region. Section 1452 of the John D. Dingell, Jr. Conservation, Management, and Recreation Act of 2019 directs the Secretary of the Interior to "assess the impacts of habitat fragmentation on wildlife within the California Desert Conservation Area," including lands managed by the Bureau of Land Management (BLM), and to "establish policies and procedures to ensure the preservation of wildlife corridors and facilitate species migration." The Act requires a study of the impact of habitat fragmentation on key species, focusing on the conservation of movement corridors that ensure connectivity across public lands within the CDCA.

In 2021, Conservation Science Partners developed a set of connectivity models identifying important movement habitat and potential corridors for six sensitive wildlife species in the CDCA under four management scenarios (hereafter referred to as the "Phase I analysis"; Conservation Science Partners 2021). These management scenarios considered the effects of increased renewable energy development and changes in the intensity of use and/or manageability of off-highway vehicle (OHV) recreation and Department of Defense (DoD) lands on species' connectivity. The present report describes a major update to the Phase I analysis wherein we have (1) expanded the suite of focal species considered; (2) substantially improved our ability to estimate the impacts of roads (including consideration of existing crossing points along major roadways), future solar development, OHV activity, and DoD activity on species movement; and (3) refined our management scenarios to increase their applicability to current and potential future conditions throughout the CDCA. In this report, we draw heavily on information originally presented in the Phase I analysis report, identifying major updates to the analysis where applicable, and referring readers back to the Phase I report for additional details where necessary.

Our principal goal for both Phase I and Phase II of this work was to identify areas of regional-scale potential connectivity for each of the focal species, i.e., connectivity based on underlying habitat suitability and the intensity of human land use. This approach prioritizes the 'best' movement options

for maintaining broad landscape connectivity and considers pathways that are suitable based on habitat conditions, which may in some cases differ from the movement routes that are most heavily used by a given focal species. Our regional focus provides a broad overview of important movement pathways across the CDCA, but may not directly account for some highly localized landscape features that potentially influence animal movement. Results should be interpreted with this in mind. Further guidance on the uses and limitations of this analysis is provided in Section 4 of this report.

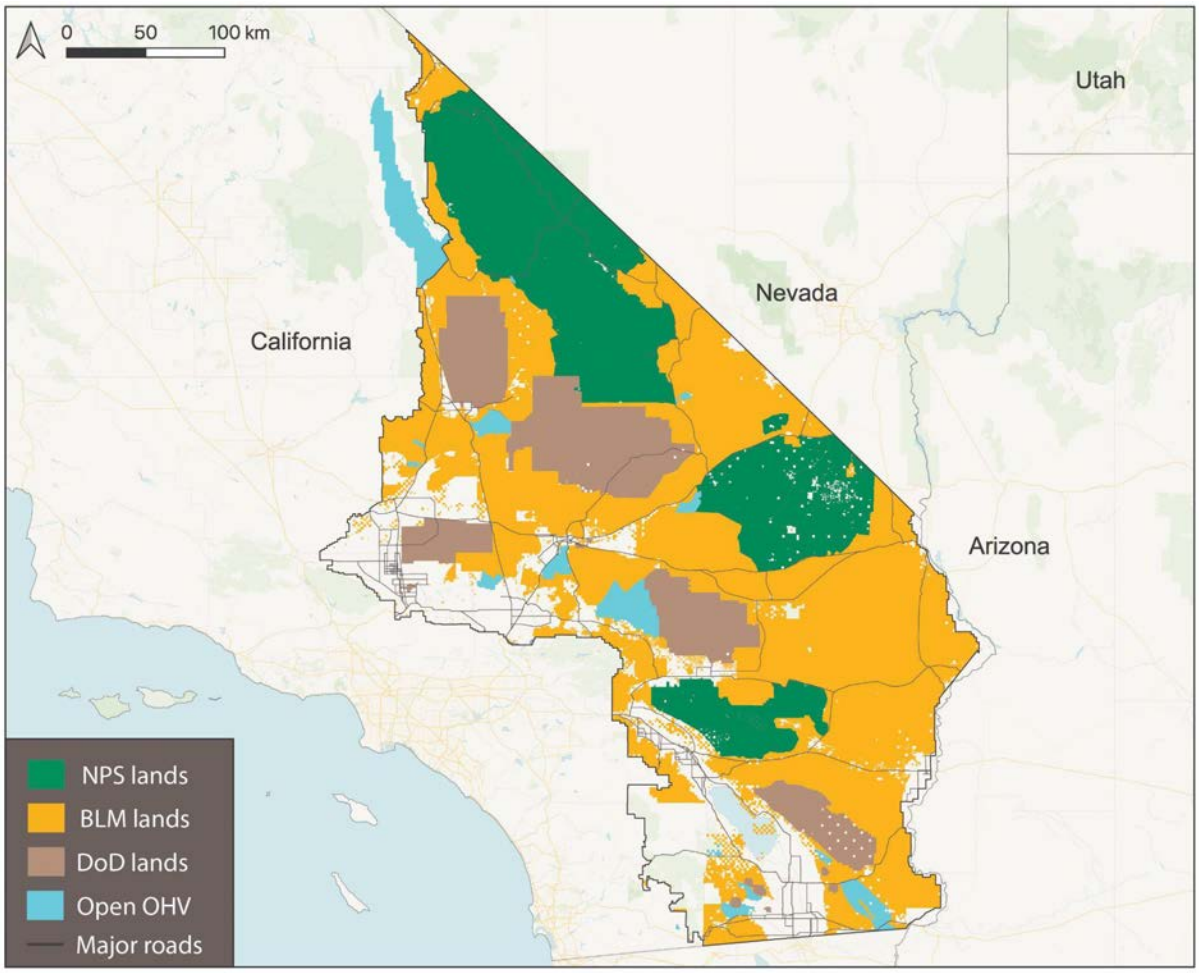

Figure 1. Map of the California Desert Conservation Area (CDCA; outlined in black), showing major ownerships and land use types, including National Park Services lands (NPS; green), Bureau of Land Management lands (BLM; orange), Department of Defense lands (DoD, brown) and open use off-highway vehicle areas (Open OHV; blue). Major roads, including highways and principal and rural arterial roads, are shown as thin gray lines.

2. METHODS

2.1 Focal species

Through consultation with managers at BLM and USFWS, we identified a suite of seven focal species to include in the connectivity analyses, based on several criteria: (1) sensitivity to energy development, recreational activity, and other human impacts; (2) management importance (e.g., species of conservation concern); (3) whether the species represented a unique functional group; (4) whether the

species could potentially serve as a proxy for important plant species (e.g., seed dispersers, habitat specialists); and (5) the availability of existing species location data and/or habitat suitability models for the CDCA region. In the Phase I analysis we focused on six species: Mojave desert tortoise (*Gopherus agassizii*, hereafter MDT), desert bighorn sheep (*Ovis canadensis nelsoni*, DBS), Mohave ground squirrel (*Xerospermophilus mohavensis,* MGS), desert kit fox (*Vulpes macrotis arsipus*, DKF), flat-tailed horned lizard (*Phrynosoma mcallii*, FTHL), and LeConte's thrasher (*Toxostoma lecontei*, LCTH). In Phase II, we include an additional focal species, mule deer (*Odocoileus hemionus*, MD), for which we developed novel habitat suitability and connectivity models, as described below.

2.2 Modeling summary

For each focal species, we first defined a study area as the intersection between the species' range and the CDCA, buffered by 100 km[1]. Including a 100-km buffer around the CDCA allows models to account for the influence of habitat outside of the CDCA on movement within it, thus minimizing edge effects. For each species, we estimated habitat suitability (from species distribution or other models, see below) and derived a spatially continuous map of the relative habitat suitability for each location on the landscape. We modeled potential connectivity using a circuit-theoretic approach, which evaluates the contributions of multiple connectivity pathways between any two points on the landscape (McRae et al. 2008). In a circuit-theoretic approach, animal movement is abstracted as current flow in a two-dimensional network of sources and resistors, with each component corresponding to a pixel in a raster representation of the landscape. As the terms imply, sources are analogous to locations from which animal movement originates (and ends) while resistance determines the difficulty an animal experiences in moving through a particular location on the landscape (McRae et al. 2008). The source strengths and resistance values, and the spatial arrangement of sources and resistors, determine current flow. A higher current flow through a given pixel corresponds to a higher probability of that pixel being used by moving animals.

We used the Omniscape algorithm (McRae et al. 2016, Landau et al. 2021), a moving-window implementation of the Circuitscape connectivity modeling package (McRae et al. 2008, Anantharaman et al. 2020), to predict and map omnidirectional landscape connectivity for each focal species. Omnidirectional approaches differ from more traditional "core" based approaches (in which connectivity is evaluated between pairs of discrete habitat patches) by evaluating connectivity between every possible pair of start and end points within a specified maximum distance of each other, and summing the results to predict cumulative current flow. In this approach, the strength of the sources of animal movement can be made to vary continuously in space based on the characteristics of each pixel (e.g., habitat suitability). A higher source strength results in greater current flow through the paths between those points.

Omniscape requires two key inputs: a source strength surface that describes the likelihood of animal movement emanating from each pixel on the landscape, and a resistance surface, which provides, for every pixel, a measure of how difficult that pixel is for the focal species to traverse. For each focal

[1] For the Mojave desert tortoise, we used its entire range as the study area, as the results may be relevant for resource managers outside of the CDCA.

species, we used the habitat suitability map as the source strength surface for connectivity models and estimated landscape resistance to species movement using a combination of habitat suitability and information on human land use and disturbance. Pixels with a high habitat suitability score received a greater amount of electrical current in our source strength surface under the assumption that movement is more likely to originate from areas of higher suitability. To quantify resistance, we combined spatial data on habitat suitability with data on human land use intensity as described below.

Following the Omniscape connectivity analysis, we delineated corridors for each focal species using random least cost paths. For each species, we calculated random least cost paths through their respective resistance surface with path start and end points determined by habitat suitability. We generated 1000 least cost paths for each species to approximate the spatial distribution of potential movement pathways. We then buffered the least cost paths by two kilometers and used the number of overlapping paths as an estimate of corridor importance in each section of the corridor network. Finally, we combined corridors from all six focal species to map multispecies corridors, quantifying the number of species predicted to use a given multispecies corridor as well as multispecies corridor importance.

2.3 Habitat suitability models

2.3.1 Models carried over from the Phase I analysis

Habitat suitability models for several focal species (MDT, DBS, MGS, FTHL, and LCTH) were carried over from the Phase I analysis, and our approach to developing those models is described in detail in the Phase I report (Conservation Science Partners 2021; see Section 2.3 and Appendix A therein). Briefly, we drew upon existing habitat models for the CDCA region for two focal species (MDT and DBS). MDT habitat suitability was based on a model by McClure et al. (2020), who used a Bayesian logistic regression approach to model the relative probability of tortoise occurrence across the Mojave desert based on tortoise location data and random pseudo absences. DBS habitat suitability was based on work by Epps et al. (2005) (see also Epps et al. 2007, Creech et al. 2017) who identified patches of occupied bighorn habitat throughout the Mojave Desert and Death Valley. These occupied patches constitute discrete mountain ranges interspersed in a matrix of non-habitat lowlands, with mountaintop patches representing separate sub-populations linked by relatively infrequent dispersal (Creech et al. 2017).

For MGS, FTHL, and LCTH, we derived species distribution models based on species observation data in the CDCA, with data provided by multiple sources. For MGS, point occurrence data were provided by Dr. Rich Inman and corresponded to those described in Inman et al. (2013), collected between 1970 and 2011. Data on FTHL occurrences were obtained from the FTHL Interagency Coordinating Committee (ICC) and correspond to the data described by Hollingsworth et al. (2017), with additional observations through 2020 (date range of observations: 2003-2020). To model LCTH habitat suitability, we used data from eBird (https://ebird.org), a citizen science-based bird observation network (Sullivan et al. 2009, Johnston et al. 2021), with data consisting of bird counts (i.e., number of individuals observed in a given location, including zero counts for unobserved species) taken between 2005 and 2020. We developed species distribution models for these three species using methods appropriate to the species and the available datasets. For MGS, we used log-gaussian cox process models, a type of point-process model

appropriate for presence only data (Renner et al. 2015). For FTHL, we used a Bayesian logistic regression approach similar to that taken for desert tortoises by McClure et al. (2020). Finally, for LCTH we used a negative binomial hurdle model appropriate for count data (Zuur et al. 2009). Full details of the species distribution models developed for MGS, FTHL, and LCTH, including model covariates, estimates of model performance, and results for each species, are provided in the Phase I report (Conservation Science Partners 2021).

2.3.2 New habitat suitability models

For the present (i.e., Phase II) analysis, We developed new habitat suitability models for two focal species, MD and DKF (with the DKF model building on work conducted during Phase I). For MD, we acquired detection and location data from a range of sources, with all deer data originating from within a 50 km buffer around the CDCA. MD data sources included: (1) helicopter surveys conducted by the California Department of Fish and Wildlife (CDFW) between 1991 and 2019 (59 detections), (2) MD occurrence records (833 records in total) compiled by the Global Biodiversity Information Facility (GBIF) between 2003 and 2022 (GBIF.org 2022), (3) VHF collar data collected from 52 individual deer (4,013 total locations) from the Imperial County deer herd between 1999 and 2004 (Marshal et al. 2006), and (4) VHF and GPS collar data collected by CDFW from 125 individual deer (20,372 total locations) in California's Peninsular Range between 2001 and 2007. Given the range of data sources and varying data density across the study area, we standardized and spatially subsampled the compiled MD dataset (using a procedure described in detail in Appendix A, Section A1), resulting in a total of 859 deer observations. These observations were paired with 7,677 background locations and used to model MD habitat suitability via logistic regression under a presence-background modeling framework (Phillips et al. 2009, Grimmett et al. 2020). Full details of the MD habitat suitability analysis are provided in Appendix A, Section A1.

We chose to rerun the DKF analysis to improve our handling of model coefficients relative to the Phase I analysis, specifically by fitting a quadratic effect of temperature to capture non-linearities in DKF temperature habitat preferences.DKF models were developed using location data obtained from iNaturalist, a citizen science database of species observations (https://www.inaturalist.org/). We eliminated all observations with missing or unavailable coordinates, as well as those that fell outside of the study area. This resulted in a total of 123 DKF locations taken predominantly between 2004 and 2021 (with two observations from 1996). These DKF observations were compared to random background locations using a logistic regression approach. This approach, along with full habitat suitability modeling details, are described in Appendix A, Section A2.

2.4 Connectivity model inputs

2.4.1 Landscape resistance surfaces

Our preparation of resistance surfaces closely follows the methods developed in the Phase I analysis, allowing comparison between Phase I and Phase II connectivity scenarios. For the set of species for which we developed species distribution models (i.e., MGS, FTHL, DFK, LCTH, and MD), initial resistance surfaces were created by integrating the resulting maps of habitat suitability for the study area with

existing spatial data on human land use intensity circa 2017 (CSP 2019). For a given species, we rescaled the habitat suitability surface to 0-1 and took the complement (i.e., subtracted from 1) to convert suitability to resistance on a 0-1 scale (R_{01}). We then calculated "habitat resistance", R_H, by rescaling R_{01} to range between 1 and a predetermined maximum value, R_{max}, using

$$R_H = R_{01} * (R_{max} - 1) + 1$$

such that the "worst" locations on the landscape are R_{max} times more resistant to movement than the "best" locations. We set R_{max} to 1000 so that resistance could approach extreme values as habitat suitability becomes worse. This rescaling resulted in a range of resistance values matching that used in other connectivity analyses employing landscape modification-based approaches (Dickson et al. 2017, Suraci et al. 2022).

We then calculated the final resistance layer by incorporating human land use intensity, *L*, using an existing dataset that integrates 12 variables on human land use into four disturbance categories - urban, transportation, energy infrastructure, and agriculture - providing an estimate of *L* that ranges between 0 and 1. Estimates of land use intensity were derived following the procedure originally described by Theobald (2013), and full details of this approach and the existing dataset are provided in CSP (2019). Here, we focused on a subset of these data corresponding to urban, energy, and agricultural land uses, excluding transportation stressors in the *L* layer, as we account for roads directly via TIGER roads data (see below). We additionally integrated updated data on existing solar footprints (from Dunnett et al. 2020, supplemented with footprints provided by the National Audubon Society), which were given a maximum *L* value of 1 (i.e., equivalent to the most heavily developed landscapes). We raised *L* to the second power so that pixels with higher land use intensity would be more strongly penalized (via higher resistance) relative to pixels with low land use intensity (following the logic of Dickson et al. (2017)). We then rescaled *L* to derive "land use resistance", R_L, using

$$R_L = L^2 * L_{scale} * R_{max}$$

where L_{scale} is a multiplier that defines the maximum resistance from *L* relative to the maximum value of habitat resistance, R_{max}. We set L_{scale} to 2, such that the maximum resistance value for R_L would be $2*R_{max}$. This results in human modification having a heavier weight on overall resistance, and results in current flow concentrating in more natural areas and avoiding human modified areas.

For MDT and DBS, we utilized and built on existing resistance surfaces as inputs to our connectivity models. For MDT, we used the resistance surface from Gray et al. (2019), which was generated by relating Brownian bridge movement probabilities from tortoise movement data to environmental covariates (see also McClure et al. 2017). For DBS, we used resistance surfaces developed by Creech et al. (2017), who built landscape resistance layers based on several input variables for two bighorn sheep populations (Mojave Desert and Death Valley) based on linear regression between bighorn population genetic distance and cost distance as estimated from the resistance surface. In line with the methodological approach of Creech et al. (2017), we conducted separate analyses for the Death Valley

and Mojave Desert populations of DBS. For both MDT and DBS, we incorporated additional information on human land uses following the approach described above.

Given that a major objective of the Phase II analysis was to explore how variation in the treatment of transportation affects predicted connectivity and corridors, we made several substantial updates to the ways in which roads and railways were incorporated into resistance surfaces for each species. These updates are described in detail in Appendix B, Section B1. Briefly, information on primary, secondary, and local roads was derived from the TIGER roads database (U.S. Census Bureau 2019), and data on railway was derived from the North American Rail Lines National Geospatial Data Asset (Federal Railroad Administration 2016). Following methods developed in the Phase I analysis, road and railway line features were used to modify the resistance surface for each focal species via a species- and road type-specific resistance multiplier, which was multiplied by R_{max} and added to R_H and R_L in producing the final resistance surface. We also acquired point data on the locations of bridges (roads and railways) and culverts (roads only) and used these to reduce the resistance associated with roads and railways in those locations, allowing current to flow more easily through these potential crossing structures than over roads or railways. The degree to which a given crossing structure reduced road or railway resistance depended on structure size and focal species body size, as described in detail in Appendix B, Section B1.

Finally, we identified water bodies using the National Land Cover Database (NLCD) 2016 land cover product (Dewitz 2019) and assigned water a resistance value of $2*R_{max}$. We derived our final resistance surface for each species by summing R_H, R_L, and road/railway resistance and overwriting all water pixels with water resistance. For all species except MDT (as Gray et al. (2019) already considered urban areas in their parameterization of resistance), we set all pixels that fell within the Human Built-up and Settlement Extent (HBASE, e.g., buildings and towns (Wang et al. 2017)) polygons to "no data", thus treating developed areas as absolute barriers. This was done to facilitate the identification of corridors within manageable areas outside of heavily developed landscapes.

2.4.2 Source strength

For each species other than DBS, we used the untransformed habitat suitability map as a source strength layer and used the NLCD to mask out pixels that were unlikely to serve as sources of animal movement (water, developed areas, and crop and pastureland). For all species for which we developed habitat suitability models for this analysis (i.e., all but MDT and DBS), we thresholded the source strength layer based on observed species locations such that only those pixels with sufficiently high values could serve as sources and targets of animal movement. To determine this threshold, we first extracted the value of the source strength layer at all observed locations for a given species (i.e., those locations used in fitting the underlying species distribution model) and then calculated the 5th percentile for this range of values, i.e., the source strength value above which 95% of observed locations occurred. Defining this source strength threshold when running Omniscape connectivity models (see below) ensured that current would only flow from locations likely to actually support individuals of the target species, while accounting for potential observations of species using suboptimal habitat (i.e., the bottom 5% of observations). For MDT, we set the source strength threshold to only include pixels in the top 25% of

habitat suitability values (i.e., relatively high suitability habitat), and for DBS, the mapped habitat cores described above were treated as areas of uniform source strength.

2.4.3 Omniscape connectivity models

All connectivity models were run using the Ominscape.jl software package (Landau et al. 2021) in the Julia programming language (Bezanson et al. 2017). For each species, we used the resistance and source strength surfaces described above. Omniscape moving window size specifies the maximum distance separating two pixels that can be connected as potential start and end points for current flow. Because our focal species differ in their size, dispersal ability, and overall vagility, we used a different moving window size in Omniscape for each species based on a literature review of species-specific dispersal and movement distances (Table 1). In general, as the moving window size gets smaller, the resulting current flow map will more closely resemble the source strength surface (in our case, habitat suitability maps for each species). In the set of models presented here, we used small moving window sizes for MDT and FTHL to reflect the reliance of these low-mobility species on relatively contiguous areas of suitable habitat.

Table 1. Moving window radii used in the Omniscape connectivity models for each focal species. Where information exists, radii are based on maximum dispersal distances reported in the literature. For the reptile species (MDT and FTHL), radii were set to 1 km to reflect these species relatively low mobility and dependence on contiguous areas of suitable habitat.

Focal species	Moving window radius	Source/Justification
Mojave desert tortoise (MDT)	1 km	To reflect low-mobility "corridor resident" status (Averill-Murray et al. 2013)
Flat tailed horned lizard (FTHL)	1 km	To reflect low-mobility "corridor resident" status (Averill-Murray et al. 2013)
Mohave ground squirrel (MGS)	8 km	(Poessel et al. 2022)
LeConte's thrasher (LCTH)	8 km	(Shuford and Gardali 2008)
Desert kit fox (DKF)	40 km	(Haight et al. 2002)
Mule deer (MD)	40 km	(Pease et al. 2009)
Desert bighorn sheep (DBS)	80 km	C. Epps, pers. comm.

2.5 Corridor delineation

While Omniscape offers a holistic view of connectivity for an entire landscape, a primary goal of this analysis was to identify and delineate movement corridors that might help to guide landscape management. Our approach to delineating corridors in this analysis is identical to that developed for

Phase I of this work. We applied a graph-theoretic least-cost path (LCP) analysis using an approach that does not rely on discrete habitat cores. In traditional core-based connectivity models, connectivity is evaluated between static habitat patches, but there is often uncertainty in where landscape cores should be placed, and where and how they are delineated can have significant consequences for results (McRae et al. 2016). A key benefit of Omniscape is that it avoids this issue, offering a 'coreless' approach to modeling connectivity (McRae et al. 2016, Landau et al. 2021). Similar to core-based connectivity models, the locations of start and end points for an LCP will also influence where the path falls. Instead of imposing assumptions about where start and end points should be placed, we chose to introduce these points stochastically by computing LCPs with random start and end locations, accounting for uncertainty about where paths should start and end. The probability for any given pixel to be selected as a start or end point was set to be proportional to its source strength used in Omniscape, such that more start and end locations are placed in pixels with higher habitat suitability. To generate a single LCP, random start and end points are sampled, then the LCP between the two is computed based on landscape resistance. With many random paths computed, the broader probability distribution of LCPs can be visualized for the entire landscape.

For the LCP analysis, we used the same inputs that were used for Omniscape connectivity modeling: a source strength map and a resistance surface. Results from Omniscape offer information on the regions within the landscape that will experience the most intense degree of movement and/or gene flow. To allow this information to inform our LCP results, we restricted the regions that could be traversed by LCPs using the cumulative current map output from Omniscape. Such an approach ensures that LCPs will not go through areas that are expected to experience limited or no movement based on the Omniscape results. However, we still wanted to allow paths to traverse narrow barriers such as roads or marginal habitats that may have had low current flow predicted by Omniscape, but are still nonetheless passable by animals. To do this, we first smoothed the cumulative current map for each species using a moving window average with a radius of 30 pixels (2.7 km). We then created a mask surface by thresholding the smoothed current map at its 25th percentile, setting pixels with values greater than the percentile to one, and pixels less than the percentile to zero. Finally, prior to generating random points and calculating LCPs, we masked the source strength and resistance surfaces using the current flow-based mask surface. Pixels where the mask was equal to zero were set to no data (i.e. infinite resistance and zero probability of being selected as a start or end point for LCPs), and pixels where the mask was equal to one retained their source or resistance values. We only allowed start and end points for least cost paths to fall within the top 25% of source strength values to prevent least cost paths from starting or ending in non habitat. For each species and each scenario, we generated 1000 least cost paths to approximate the spatial distribution of potential movement corridors. We then buffered each path by two kilometers to create an individual corridor for each path. We chose this corridor width to be wide enough to visualize the general locations of corridors in place, and encourage the use of current flow maps (representing connectivity) in conjunction with corridors to understand how species are likely to move within and around the corridors. Additional guidance on the combined use of corridor and current flow maps is provided in Section 4.1. Finally, we overlapped the 1000 corridors, and for each unique polygon in the intersection, we counted the number of overlapping least-cost corridors. The more LCPs that go through a given polygon (which can be considered a node in a graph), the more central that polygon is to the

connectivity of the entire network (Newman 2005). Thus, the betweenness centrality (hereafter, centrality) for a given section in the corridor network can be approximated by the number of paths that go through that section. For all species except the FTHL, we only retained sections of the corridor networks that had at least 10 overlapping corridors (i.e. 1% of the 1000 LCPs generated). For the FTHL, because of its small geographic range, we only retained sections that had at least 15 overlapping paths. Following this filtering, we manually removed small polygons that became isolated from the larger network of paths as a result of the filtering step.

For each scenario, we created two multispecies corridor maps: a corridor centrality map, and a map describing the number of species predicted to use each section of the multispecies corridor network. To obtain the corridor centrality map, we intersected the filtered corridor networks for each species and calculated the total number of corridors for all species passing through each polygon in the intersection. This estimate of centrality does not account for the total number of focal species predicted to use a section of the network, but simply quantifies the total number of overlapping least cost paths across all species. To create our map describing the number of species using each section of the multispecies network, we first dissolved the geometries of the filtered corridor networks for each species. We then intersected the dissolved boundaries of each species' corridor network and calculated the number of overlapping polygons (which corresponds to the number of focal species).

2.6 Management scenarios

In collaboration with natural resource managers from BLM and FWS, we developed a set of four scenarios to quantify and map connectivity under current conditions in the CDCA, as well as under hypothetical future conditions that account for increases in renewable energy development and OHV activity and expanded activity on DoD installations. We formulated the scenarios by modifying the human land use intensity layer (*L* above, which ranges between 0 and 1) used to derive resistance surfaces, incorporating additional landscape features representing barriers to movement and adjusting the human land use intensity value assigned to these features for different scenarios. For most species, we also adjusted the habitat suitability and source strength layers based on scenario assumptions (as described below) to reflect reduced movement to and from areas affected by modeled human impacts. For the desert bighorn sheep, because source strength layers were based on discrete patches rather than continuous values, and because these discrete patches tended to fall outside of areas heavily impacted by human land use, we did not alter source strength for any of the scenarios. For each species and scenario, we then recalculated resistance and/or source strength and subsequently reran Omniscape and corridor models using the updated inputs for the relevant scenario. We then developed multispecies corridors for each scenario as described in Section 2.5 above.

We acquired spatial data on individual barriers to movement in the CDCA from several sources. For OHV activity, we acquired line data on OHV trails throughout the CDCA from the OwlsheadGPS Project Phase II, available on the Desert Renewable Energy Conservation Plan (DRECP) Base Layers dataset on DataBasin (https://drecp.databasin.org/), as well as additional trail data from the WEMO OHV dataset, provided directly by BLM staff. OHV trail line data were converted to an OHV trail density surface using Google Earth Engine's reduceNeighborhood() function, a moving window smoother. We used a Gaussian

kernel with a standard deviation of 270 meters and a maximum radius of 1080 meters, which calculated the weighted proportion of each moving window that contained OHV tails. The resulting trail density layer ranged in value from zero to one, where a value of one is reached for a given pixel only if every pixel within the surrounding Gaussian kernel is intersected by an OHV trail. OHV activity also occurs in "open areas" on BLM land, and we acquired vector data on the boundaries of open OHV areas (including Imperial Sand Dunes and Johnson Valley OHV areas) from the DRECP DataBasin site. OHV activity is essentially permitted anywhere within the boundaries of open areas, though in practice, activity is likely to be concentrated within certain sections of a given open area due to, e.g., terrain constraints. As described in detail in Appendix B, Section B2, we used a computer vision model trained on high-resolution aerial imagery from across the CDCA to classify landscape pixels within each open use area into one of four OHV route density categories: no OHV routes, one route, two-to-three routes, or four or more routes.

We estimated military maneuver intensity (e.g., weapons training, motor vehicle operation) on two DoD installations, Fort Irwin and the Marine Corp Air Ground Combat Center at Twentynine Palms (MCAGCC), the two most intensively used military bases in the CDCA. Our procedure for estimating maneuver intensity is described in detail in Appendix B, Section B3, and relied on (1) DoD-reported spatial information on "off-limits areas" (i.e., areas where no maneuvers are conducted) and (2) slope of the terrain. Maneuver intensity estimates were grouped into five categories and assigned *L* values between 0 and 0.5, which were then added to the baseline *L* layer. We developed two maneuver intensity surfaces based on both present day and anticipated future maneuver intensities (see Appendix B, Section B3 for details).

Under the DRECP, three land categories are designated for potential future renewable energy development: Development Focused Areas (DFAs) and Variance Process Lands (VPLs) are available for relatively intensive levels of renewables development (with development incentivized on DFAs), while General Public Lands (GPLs) are available for more moderate levels of development. We acquired data on the boundaries of all three land designations from the DRECP DataBasin site. Solar development is required to avoid sensitive habitats within DFAs, VPLs, GPLs, specifically sand dunes and microphyll woodlands. We acquired data on sand dunes from the DRECP DataBasin site and developed a novel layer for microphyll woodlands, as described in Appendix B, Section B4. Sand dunes and microphyll woodlands were then combined into a "sensitive habitat" layer and used as described in the scenarios below. We modeled connectivity for each focal species under the following four scenarios:

SCENARIO 1: PRESENT DAY - MINIMALLY PERMEABLE ROADS & RAILWAYS

This scenario captures present conditions in the CDCA, but *ignores* potential crossing structures (bridges and culverts) along roads and railways, thus treating these linear features as minimally permeable to animal movement. We incorporated present day DoD maneuver intensity (see Appendix B) and assumed moderate levels of resistance associated with OHV activity. For OHV trails (based on line data, see above), we converted trail density to an *L* score by multiplying density by 0.4. Thus, areas with the highest OHV trail densities received *L* values comparable to those of moderately used roads in previous studies (e.g., CSP 2019). We then added the rescaled OHV trail density values to the baseline *L* layer.

Within open use OHV areas, we reassigned our four OHV route density categories to the following *L* values and added these values to the baseline *L* layer: no routes = 0, one route = 0.17, two-to-three routes = 0.33, four or more routes = 0.50.

SCENARIO 2: PRESENT DAY - MODERATELY PERMEABLE ROADS & RAILWAYS

This scenario is identical to Scenario 1 except that information on potential crossing structures (bridges and culverts) is used to modify the resistance associated with roads and railways (as described in Appendix B, Section B1). Comparison between Scenarios 1 and 2 for a given focal species (or for multispecies corridors) can be used to assess the potential effect of these crossing structures on wildlife movement and connectivity across the CDCA.

SCENARIO 3: FUTURE - MODERATE INTENSITY

This scenario builds on Scenario 2 (i.e., includes crossing structures as modifiers of road and railway resistance) and incorporates moderate levels of resistance associated with OHV activity (as described in Scenario 1). This scenario includes anticipated future impacts of DoD maneuver intensity as well as potential future solar development. Future solar development is assumed to be 'moderate' in this scenario such that GPLs and VPLs are built out to half of their maximum allowable level (as determined by the DRECP, 25% and 40% respectively), and DFAs are built out to their maximum allowable level (80%). All solar development avoids sensitive areas (microphyll woodlands and sand dunes). To implement solar buildout, we followed the procedure developed in Phase I of this analysis, assigning all pixels within a given solar development polygon an *L* value corresponding to the proportion of the polygon assumed to be developed (after accounting for the avoidance of sensitive habitats). For instance, setting the *L* value for all pixels within a DFA to 0.8 is equivalent to considering that any fully developed pixel has an *L* value of 1 (i.e., maximum human modification) and that each pixel within the DFA has an 80% chance of being fully developed. We chose this approach rather than explicitly assigning individual pixels as developed or not because of uncertainty in how development will proceed within any individual polygon. In addition to modifying *L* as described above, we also modified habitat suitability within DFA, VPL, and GPL polygons for the purposes of calculating source strength. Following similar logic used for determining *L* above, we multiplied habitat quality in DFA, VPL, and GPL polygons by 1 - *L* to reflect a loss of habitat within those areas proportional to the amount of area assumed to be developed for solar.

SCENARIO 4: FUTURE - HIGH INTENSITY

This scenario builds on Scenario 3 (including bridges and culverts as well as anticipated future DoD activity), but assumes an increased intensity of OHV activity relative to present day levels as well as a higher intensity of future solar development. OHV resistance modifiers are doubled under this scenario (OHV trail density multiplied by 0.8; open OHV route density categories assigned values of 0, 0.33, 0.66, and 1). Solar development GPLs and VPLs were assumed to be built out to their maximum allowable amount (50% and 80%, respectively), with development avoiding sensitive habitats. DFAs were assumed to be fully developed (100%), regardless of the presence or absence of sensitive habitats.

2.7 Parcelization of multispecies corridor networks

A significant portion of the land within the CDCA boundary is under private land ownership or management. As a result, private lands (and landowners) will likely serve a critical role in maintaining multispecies movement corridors as decisions are made about where, when, and how intensely those areas are developed. Federal and state land management authorities may also consider land acquisitions as a tool for reducing development pressures within critical connectivity habitat. Identifying where corridor networks overlap with private lands and the degree to which those private lands consist of many small or fewer large parcels can help guide management strategies. We therefore estimated, for each management scenario, the number and average size of private land parcels segments of our multispecies corridor networks within the CDCA.

We obtained assessor's parcel spatial data for all California counties that overlap with the CDCA from county-level geospatial clearinghouses. These included Imperial, Inyo, Kern, Los Angeles, Riverside, San Bernardino, and San Diego counties. County-level datasets did not consistently report ownership type. Therefore, to identify the subset of parcels likely to be under private ownership, we downloaded the Bureau of Land Management's Surface Management Agency (SMA) geodatabase (BLM 2022) and filtered the SMA to only those lands under private or "unknown" management in California (i.e., not managed by federal or state agencies). This filtered SMA dataset was then used to subset the parcel dataset to only private or "unknown" parcels (hereafter referred to simply as private parcels). We further restricted the parcel dataset to only those private parcels that fell within the boundary of the CDCA, and then estimated the total area of each individual parcel in acres.

To estimate the degree of parcelization within high-value wildlife corridors across the CDCA, we overlaid parcel data with the multispecies corridor network developed for each scenario, focusing on the corridor datasets describing the total number of species predicted to use each segment of the corridor network. Spatially contiguous portions of the corridor network predicted to be used by the same number species were merged to create corridor segments. For each corridor segment, we estimated (1) the total number of private land parcels within the segment, (2) average size of parcels within the segment, and (3) the estimated density of parcels within the segment (i.e., number of parcels per unit area of the segment). These calculations were performed only for those corridor segments and parcels falling within the CDCA boundary and were conducted separately for the multispecies corridor network derived from each scenario.

3. RESULTS AND DISCUSSION

3.1 Single species connectivity and corridors

For each species (and the two separately-analyzed populations of bighorn sheep), we generated omni-directional current flow predictions and corridor maps for each of the four scenarios described in Section 2.6. Spatial GIS layers for all current flow and corridor maps are provided as part of the data package accompanying this report. To provide context and to aid in interpretation of these model results, here we visualize and discuss a subset of the connectivity and corridor maps for each species. In general, we strongly encourage considering both corridors and underlying connectivity maps when identifying

areas for conservation, as these products represent different but complementary information on the importance of a given area for supporting animal movement. Connectivity maps emphasize areas predicted to experience high levels of animal movement and are therefore useful in identifying high-value habitat patches that support important movement processes (e.g., dispersal). Our approach to developing corridors prioritizes maintaining connectivity across the entire network of potential movement pathways (i.e., across the entire study area for a given focal species) and thus provides a regional-scale assessment of connectivity that may overlook some locally important movement habitat. For further discussion of the joint use of corridor and connectivity maps in conservation planning, see Section 4.1 below.

Figures 1 and 2 show predicted connectivity (current flow) across the study area for two representative species under both present conditions (Scenario 2) and the high intensity future scenario (Scenario 4). DKF (Fig. 1) is a relatively mobile species (omniscape moving window radius = 40 km) with high predicted connectivity in relatively undeveloped regions of the study area in the south and east. When comparing Scenario 2 (Fig. 1a) and Scenario 4 (Fig. 1b), substantial local reductions in connectivity can be seen in Scenario 4 in areas predicted to experience increased impacts from, e.g., OHV activity (central study area near Victorville and Barstow) and future solar development (southeastern CDCA). MDT (Fig. 2) has substantially lower mobility (omniscape moving window radius = 1 km), with predicted current flow in both scenarios reflecting the distribution of suitable habitat across the region. Effects of future increases in human land use intensity on connectivity (Fig. 2b) are predicted to be relatively localized but may have a large cumulative impact across this species' range by reducing the overall footprint of suitable habitat.

Importantly, relatively modest or localized changes in current flow can have substantial effects on the resulting corridor network by shifting the trajectory of least cost movement paths across the landscape. This point is illustrated by the effect of including potential crossing structures (bridges and culverts; see Appendix B, Section B1) across major highways that were otherwise considered impermeable to MDT movement. Figure 3 compares both current flow and predicted corridors for a section of the CDCA along Highway 15 under Scenario 1 (present day conditions with minimally permeable roads and railways, i.e., no crossing structures; Fig. 3a) and Scenario 2 (present day conditions with crossing structures Fig. 3b). Without crossing structures, corridors are forced to avoid or run parallel to the highway while the inclusion of crossing structures allows corridors to cross the highway at locations where one or more structures are associated with regions of relatively high current flow. By contrast, the effects of including crossing structures on current flow itself are relatively limited given the localized nature of MDT movements.

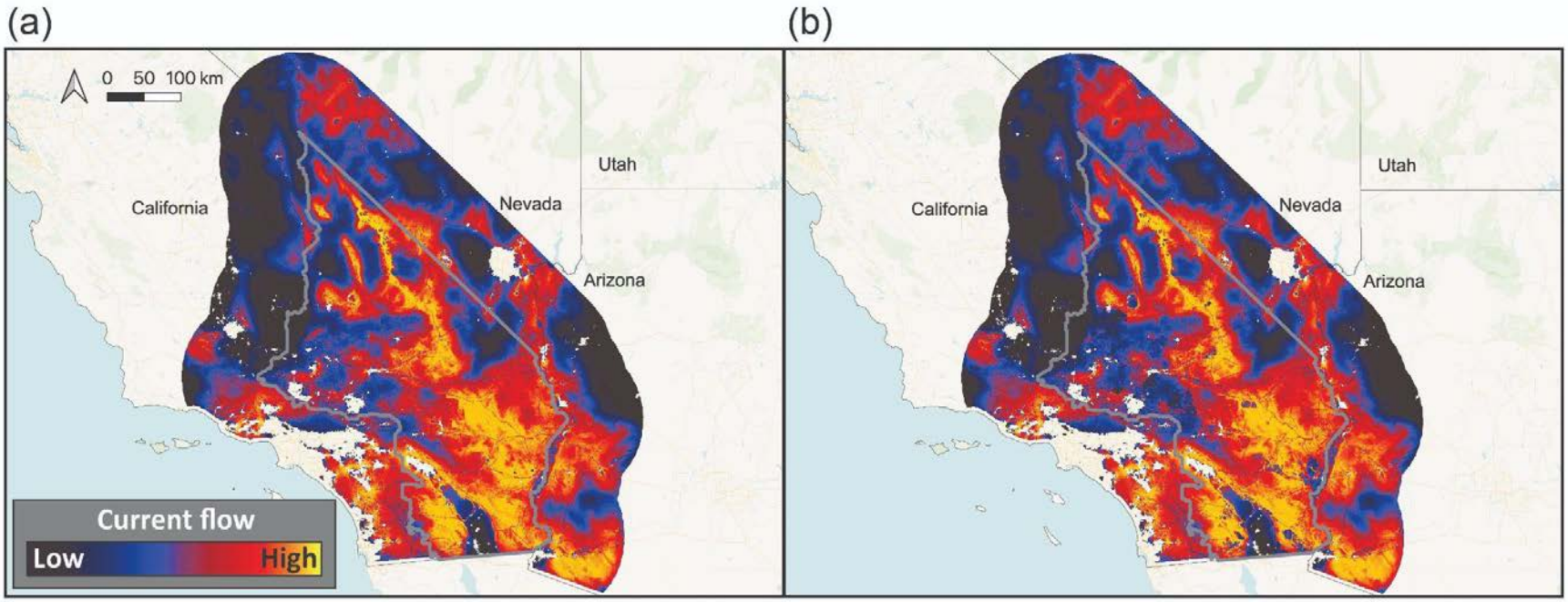

Figure 1. Map of predicted desert kit fox connectivity under the present-day scenario with moderately permeable roads and railways (Scenario 2, left) and under the (b) high intensity future scenario (Scenario 4), illustrating predicted areas of high movement (warmer colors). Connectivity is shown as cumulative Omniscape current flow. The boundary of the CDCA is shown as a gray outline.

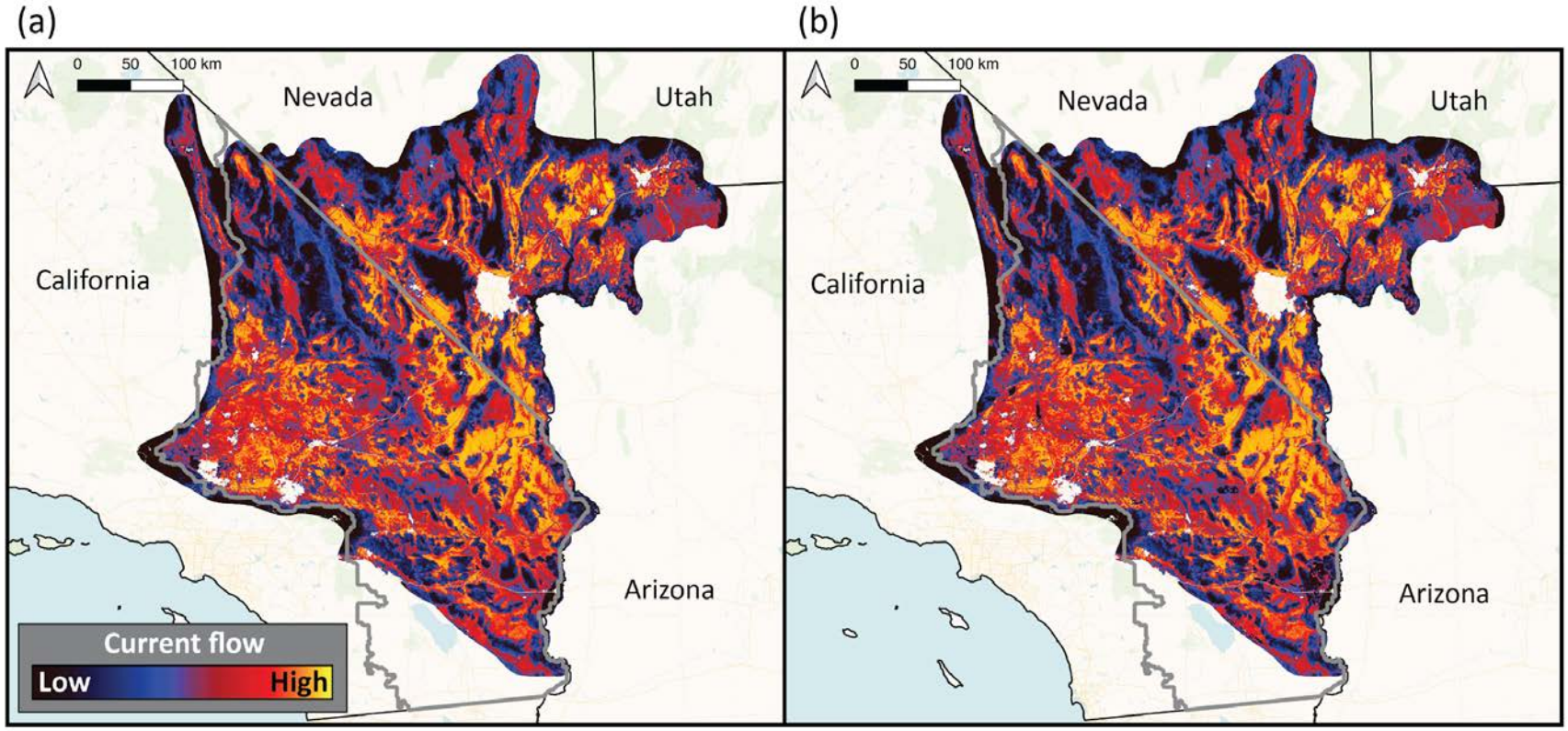

Figure 2. Map of predicted Mojave desert tortoise connectivity under the present-day scenario with moderately permeable roads and railways (Scenario 2) and under the (b) high intensity future scenario (Scenario 4), illustrating predicted areas of high movement (warmer colors). Connectivity is shown as cumulative Omniscape current flow. The boundary of the CDCA is shown as a gray outline.

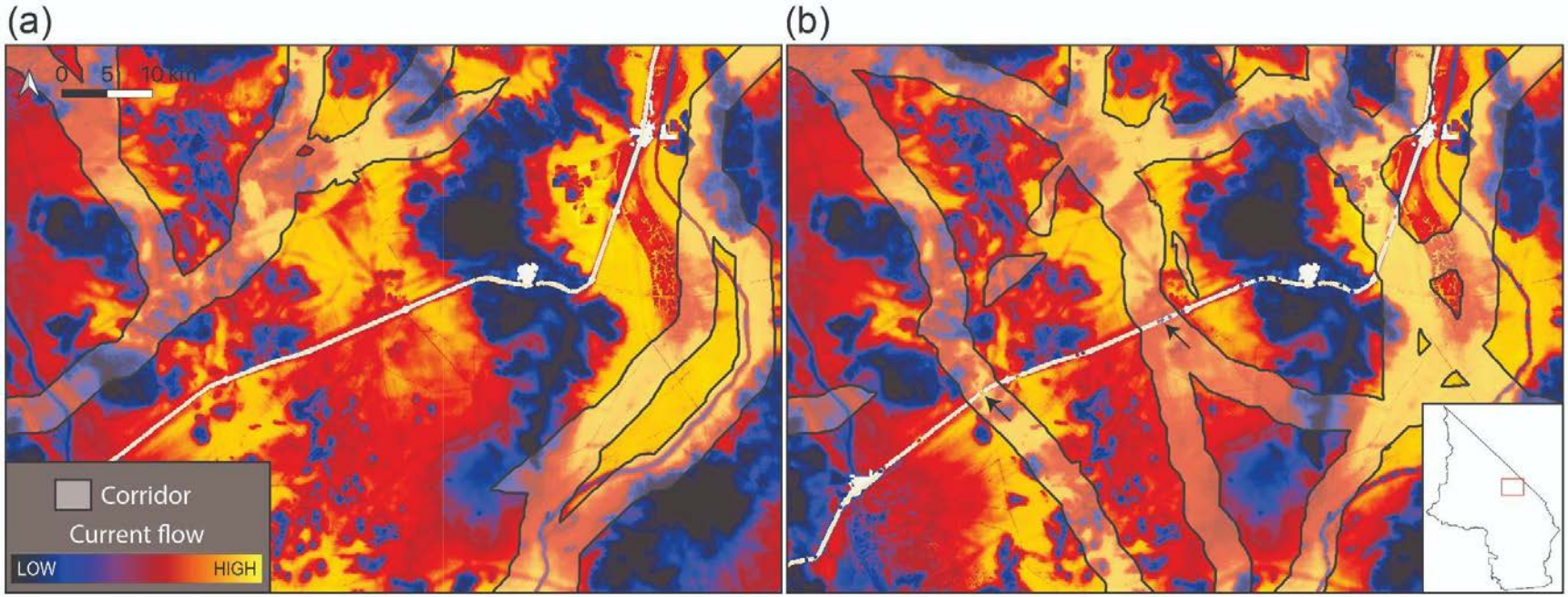

Figure 3. Detailed map of predicted Mojave desert tortoise connectivity under the two present-day scenarios with (a) minimally permeable (Scenario 1) and (b) moderately permeable (Scenario 2) roads and railways and under the high-intensity development future (Scenario 4, right) illustrating the effects of accounting for existing crossing structures (bridges and culverts) on connectivity (cumulative Omniscape current flow) and the locations of predicted corridors. Small black arrows in (b) show the locations of two crossing structures across Highway 15. The inset shows the location of the detailed area within the CDCA.

Figures 4 through 7 present MDT corridor maps for each of the four management scenarios, illustrating the effects of each of scenarios on predicted single-species corridors across the CDCA. As described in detail in Section 2.5, corridors were created by overlapping 1000 least cost paths with random start and endpoints, and as such each corridor in the resulting network represents a potentially important movement pathway for the focal species. These maps also illustrate corridor centrality, an estimate of a given corridor segment's importance in facilitating connectivity across the entire network (estimated here as the number of least cost paths passing through that segment). Corridor centrality highlights particularly critical pathways for maintaining long-term connectivity throughout the study region. For the tortoise, long, highly central, SW-to-NE trending corridors in the northern and southern portions of the study area remain relatively constant across scenarios, with one high-centrality corridor notably passing through the northern portion of Ft. Irwin, where low maneuver intensity results in relatively low resistance. Comparing Figure 4 (Scenario 1) and Figure 5 (Scenario 2) illustrates the regional scale effects of accounting for existing crossing structures across otherwise highly resistant highways, with crossing structures facilitating more (and higher-centrality) corridors through the middle of the study area crossing Highways 15 and 40. Future solar development, expanded maneuvers at MCAGCC, and OHV intensification under Scenarios 3 and 4 (Figs. 6 and 7) lead to shifts in both the spatial position and centrality of corridors in the western and southern portions of the study area, and highlight potential fragmentation of the corridor network in peripheral regions.

For all other species, we present corridor maps for Scenarios 2 and 4 to allow comparison of present day conditions with our high intensity future scenario. As in our Phase I analysis, FTHL corridors (Fig. 8) occurred in two clusters within this species' relatively restricted range in the southern CDCA, with the two clusters separated by developed areas along Highway CA-111. FTHL corridor footprint and centrality reflect the impacts of both OHV activity (with corridors avoiding portions of open OHV areas with relatively high route density) and future solar development, which is predicted to be extensive in this region of the southern CDCA. For MGS (Fig. 9), LCTH (Fig. 10), and DKF (Fig. 11), high-centrality corridors through the middle of each species' range tended to remain constant across scenarios, but the spatial footprint of the corridor network in peripheral regions shifted due to the predicted impacts of future solar development. For DBS, corridors were derived separately for the two populations considered here (the Mojave Desert and Death Valley populations). The two corridor networks were overlaid in Figure 12 to represent potential linkages both within and between populations, with potential linkages between populations occurring along the eastern edge of the CDCA. Increased future development (Fig. 12b) had relatively modest effects on the overall footprint and centrality of bighorn corridors.

MD only occupy relatively limited portions of the CDCA (see Appendix A, Fig. A1.1), with most suitable MD habitat occurring in the mountain ranges surrounding the desert region. Our modeling suggests that deer populations in the Inyo Mountains and in the Mojave National Preserve (along the CDCA's northern and eastern borders, respectively) may be relatively isolated from other desert deer populations, but identified a key set of corridors potentially facilitating connections within and among deer herds in the Peninsular Range (southwestern CDCA) and Imperial County (southeastern CDCA) (Fig. 13). Our models predict that these corridors will persist in the face of increased solar development in the southern CDCA, but that the exact spatial footprint may shift to avoid areas of heavy buildout. Our analysis also identified

a high-centrality MD corridor through the mountains along the western border of the CDCA, the middle sections of which were substantially impacted (in terms of both footprint and centrality) under the high intensity future scenario.

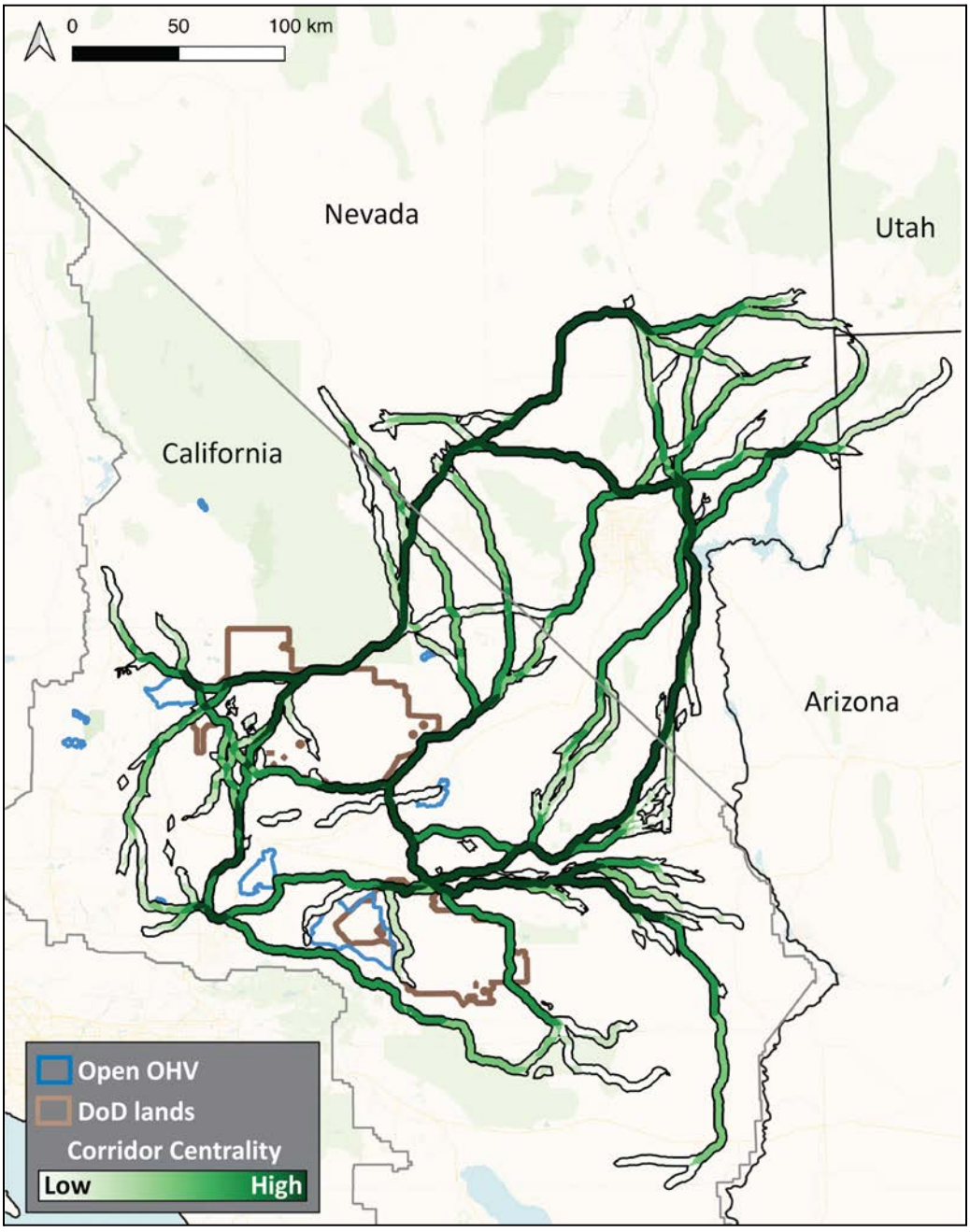

Figure 4. Map of predicted Mojave desert tortoise corridors under the present day scenario with minimally permeable roads and railways (Scenario 1). Increasing corridor centrality (i.e., the number of random least cost paths overlapping a given corridor) is indicated by darker shades of green. Open off-highway vehicle (OHV) areas (blue polygons) and major Department of Defense (DoD) installations (brown polygons) are shown for reference. This scenario also included OHV trail density, but trails are excluded here for clarity.

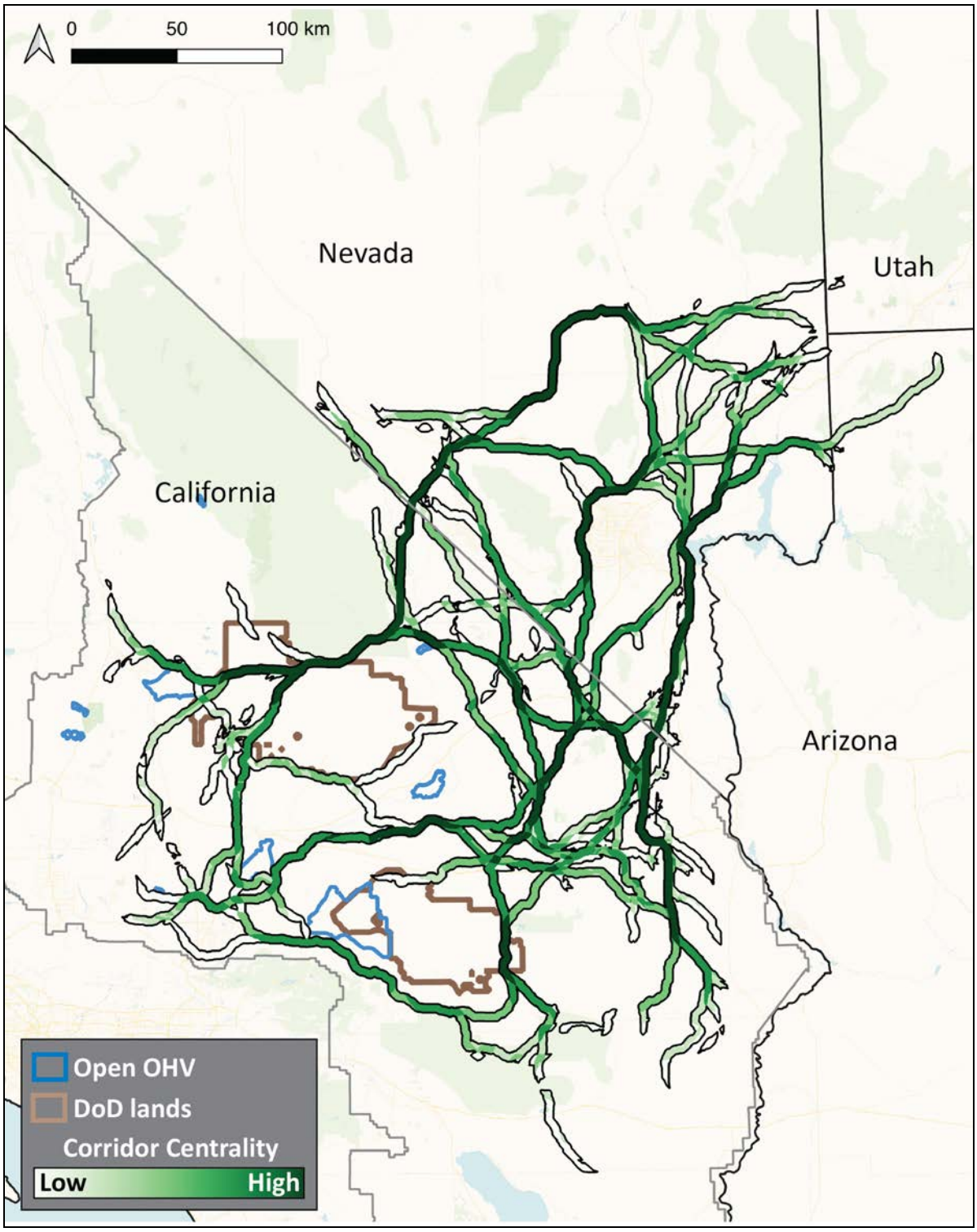

Figure 5. Map of predicted Mojave desert tortoise corridors under the present day scenario with moderately permeable roads and railways (Scenario 2). Increasing corridor centrality (i.e., the number of random least cost paths overlapping a given corridor) is indicated by darker shades of green. Open off-highway vehicle (OHV) areas (blue polygons) and major Department of Defense (DoD) installations (brown polygons) are shown for reference. This scenario also included OHV trail density, but trails are excluded here for clarity.

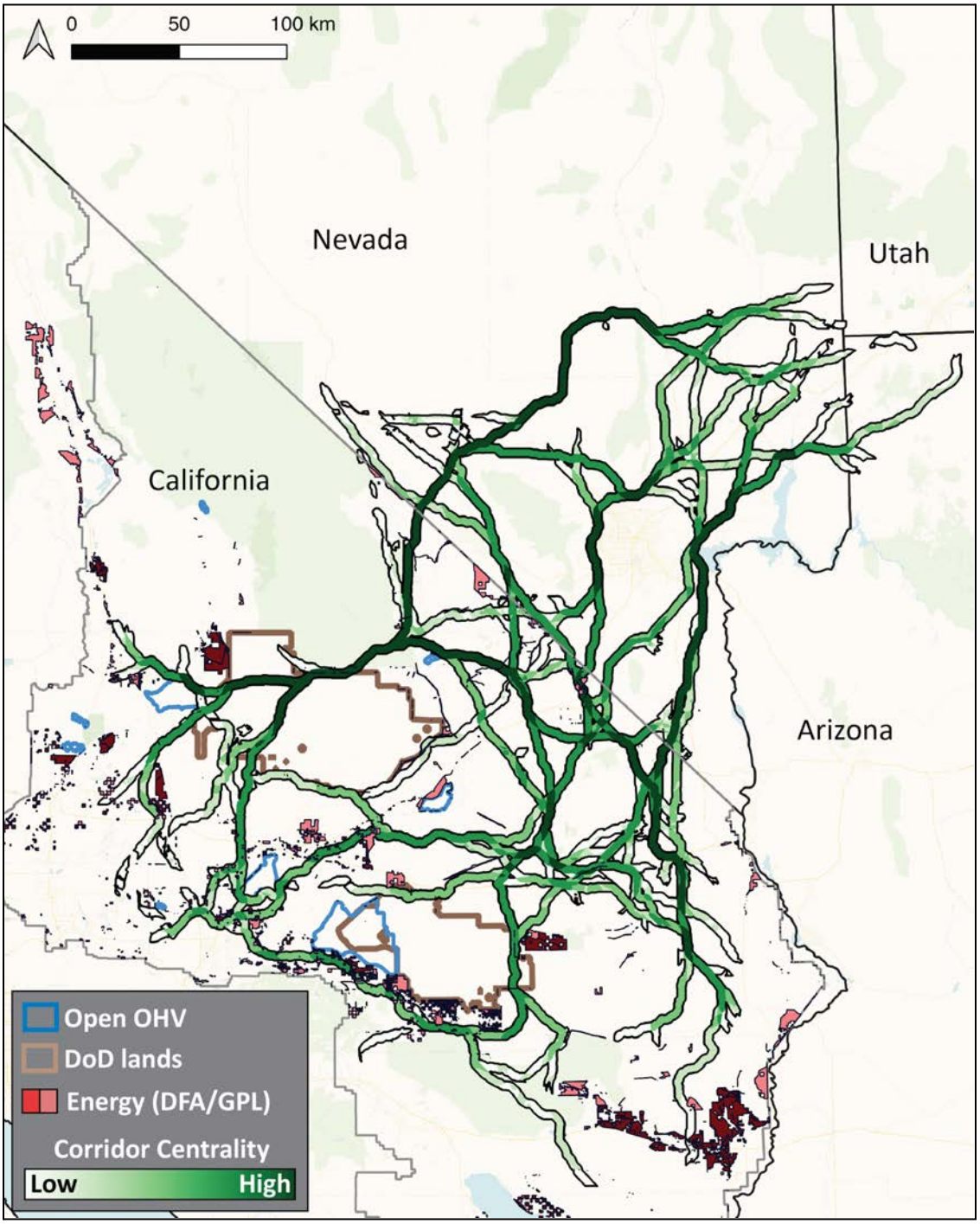

Figure 6. Map of predicted Mojave desert tortoise corridors under the moderate intensity future scenario (Scenario 3). Increasing corridor centrality (i.e., the number of random least cost paths overlapping a given corridor) is indicated by darker shades of green. Open off-highway vehicle (OHV) areas (blue polygons) and major Department of Defense (DoD) installations (brown polygons) are shown for reference. Areas authorized for future solar development are shown in shades of red, with Development Focused Areas (DFA) and Variance Process Lands (VPL) shown as dark red polygons and General Public Lands (GPL) shown as pink polygons. This scenario also included OHV trail density, but trails are excluded here for clarity.

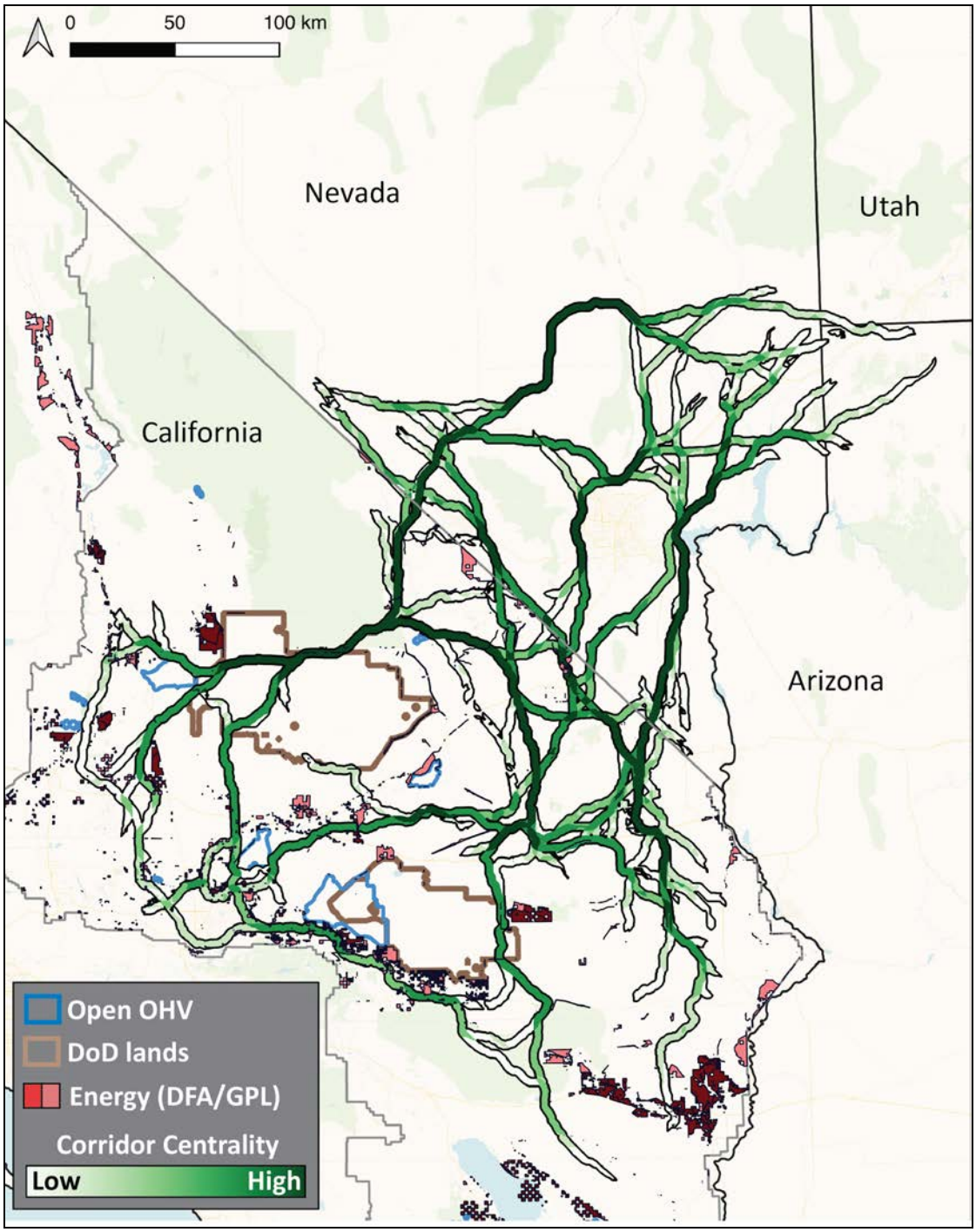

Figure 7. Map of predicted Mojave desert tortoise corridors under the high intensity future scenario (Scenario 4). Increasing corridor centrality (i.e., the number of random least cost paths overlapping a given corridor) is indicated by darker shades of green. Open off-highway vehicle (OHV) areas (blue polygons) and major Department of Defense (DoD) installations (brown polygons) are shown for reference. Areas authorized for solar energy development are shown in shades of red, with Development Focused Areas (DFA) and Variance Process Lands (VPL) shown as dark red polygons and General Public Lands (GPL) shown as pink polygons. This scenario also included OHV trail density, but trails are excluded here for clarity.

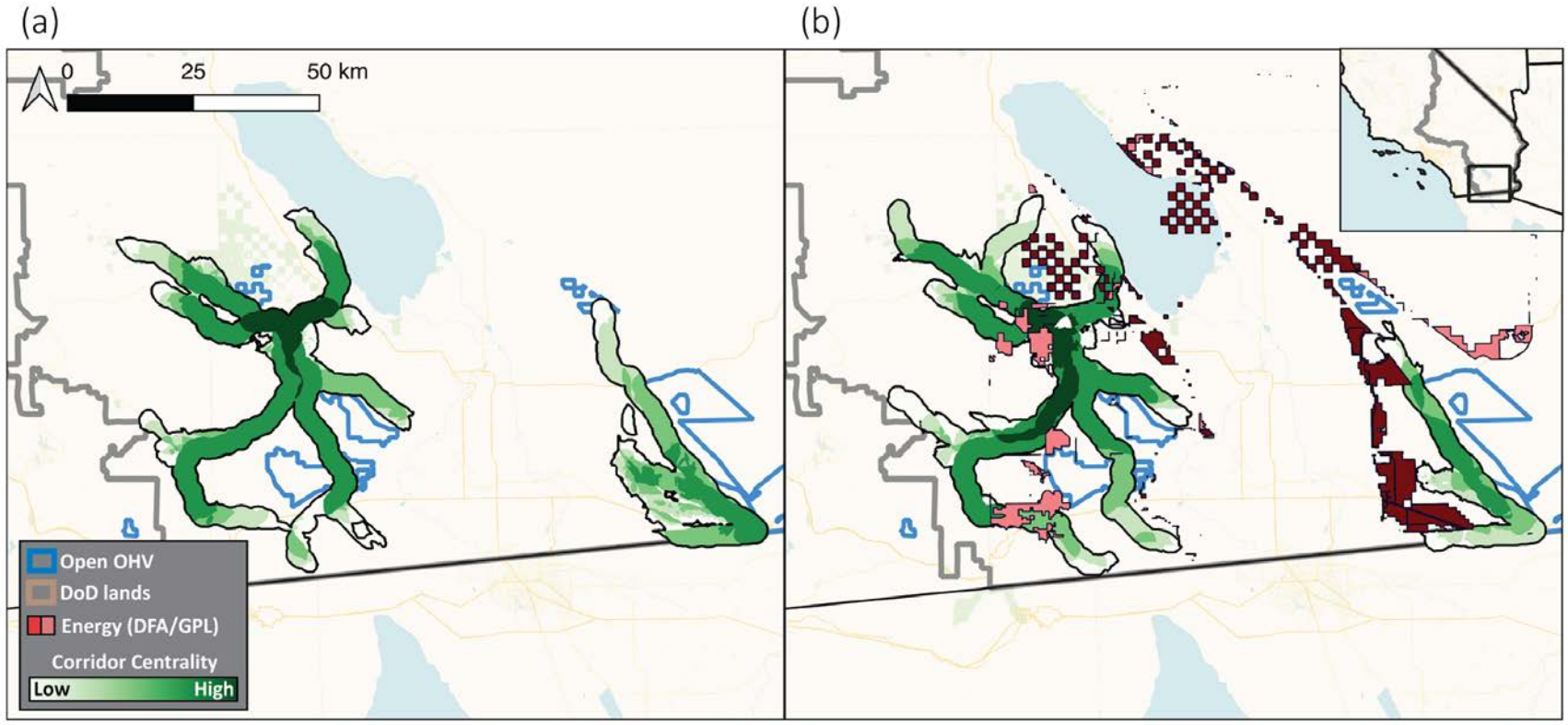

Figure 8. Map of predicted flat-tailed horned lizard corridors under (a) the present day scenario with moderately permeable roads and railways (Scenario 2) and under (b) the high intensity future scenario (Scenario 4). Increasing corridor centrality (i.e., the number of random least cost paths overlapping a given corridor) is indicated by darker shades of green. Open off-highway vehicle (OHV) areas (blue polygons) and major Department of Defense (DoD) installations (brown polygons) are shown for reference. Areas authorized for solar energy development are shown in shades of red, with Development Focused Areas (DFA) and Variance Process Lands (VPL) shown as dark red polygons and General Public Lands (GPL) shown as pink polygons. Both scenarios also included OHV trail density, but trails are excluded here for clarity.

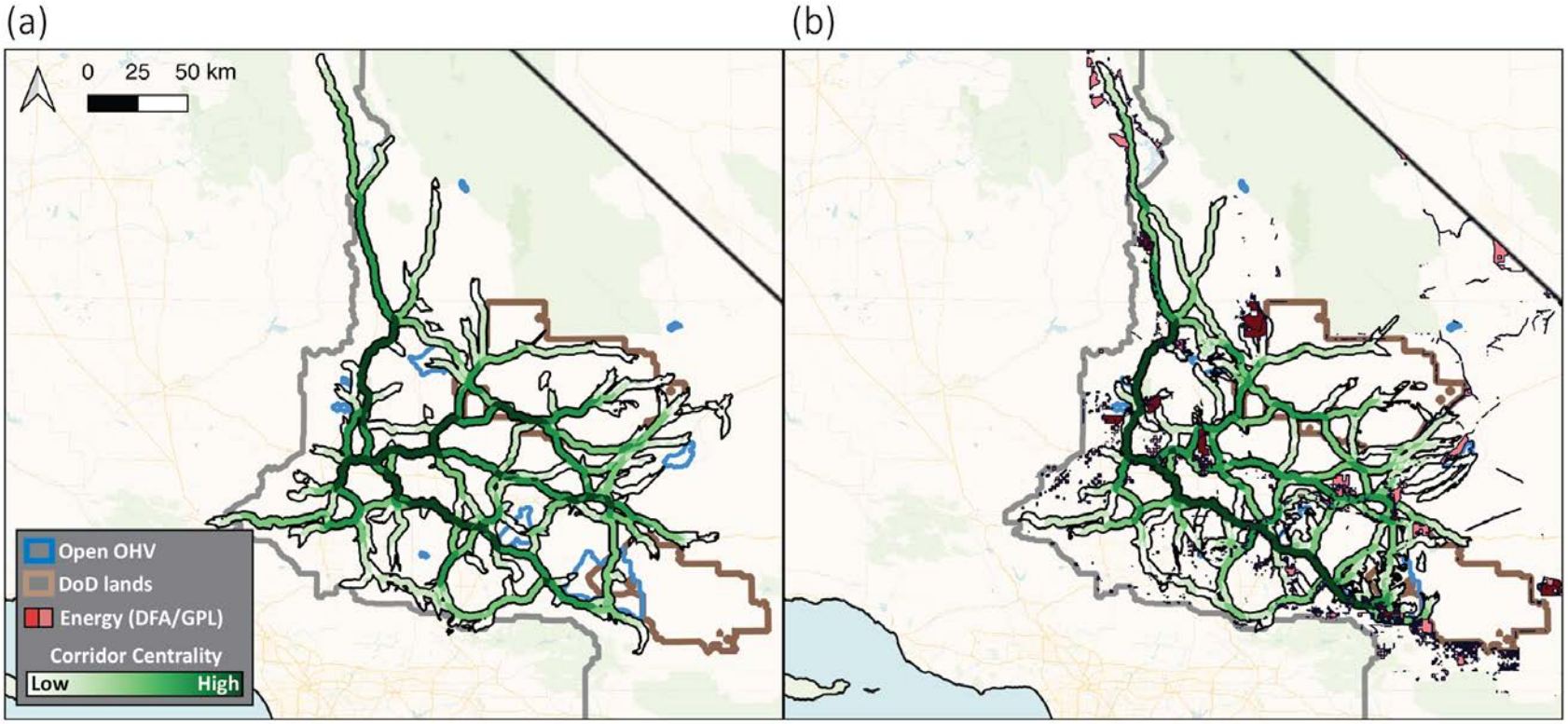

Figure 9. Map of predicted Mohave ground squirrel corridors under (a) the present day scenario with moderately permeable roads and railways (Scenario 2) and under (b) the high intensity future scenario (Scenario 4). Increasing corridor centrality (i.e., the number of random least cost paths overlapping a given corridor) is indicated by darker shades of green. Open off-highway vehicle (OHV) areas (blue polygons) and major Department of Defense (DoD) installations (brown polygons) are shown for reference. Areas authorized for solar energy development are shown in shades of red, with Development Focused Areas (DFA) and Variance Process Lands (VPL) shown as dark red polygons and General Public Lands (GPL) shown as pink polygons. Both scenarios also included OHV trail density, but trails are excluded here for clarity.

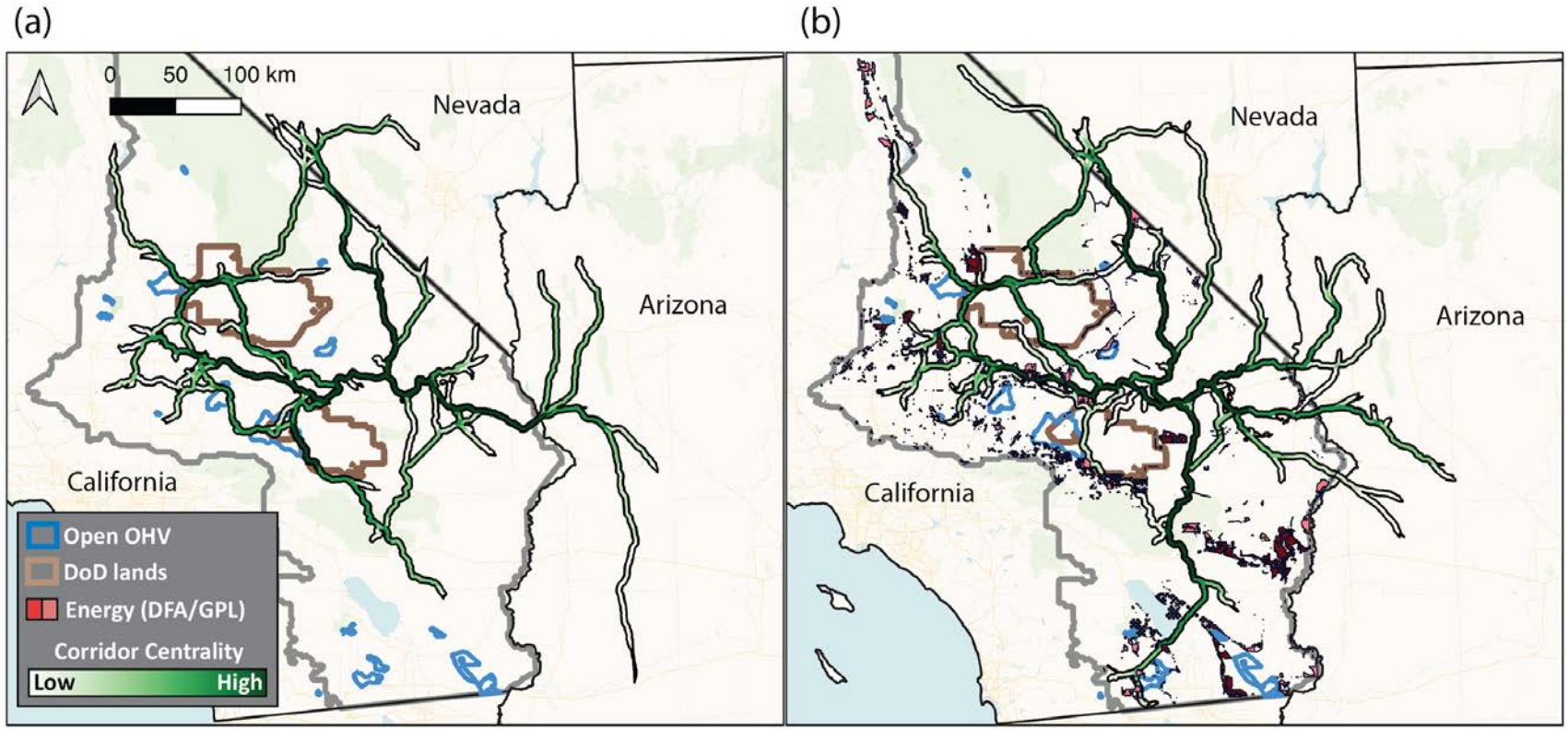

Figure 10. Map of predicted LeConte's thrasher corridors under (a) the present day scenario with moderately permeable roads and railways (Scenario 2) and under (b) the high intensity future scenario (Scenario 4). Increasing corridor centrality (i.e., the number of random least cost paths overlapping a given corridor) is indicated by darker shades of green. Open off-highway vehicle (OHV) areas (blue polygons) and major Department of Defense (DoD) installations (brown polygons) are shown for reference. Areas authorized for solar energy development are shown in shades of red, with Development Focused Areas (DFA) and Variance Process Lands (VPL) shown as dark red polygons and General Public Lands (GPL) shown as pink polygons. Both scenarios also included OHV trail density, but trails are excluded here for clarity.

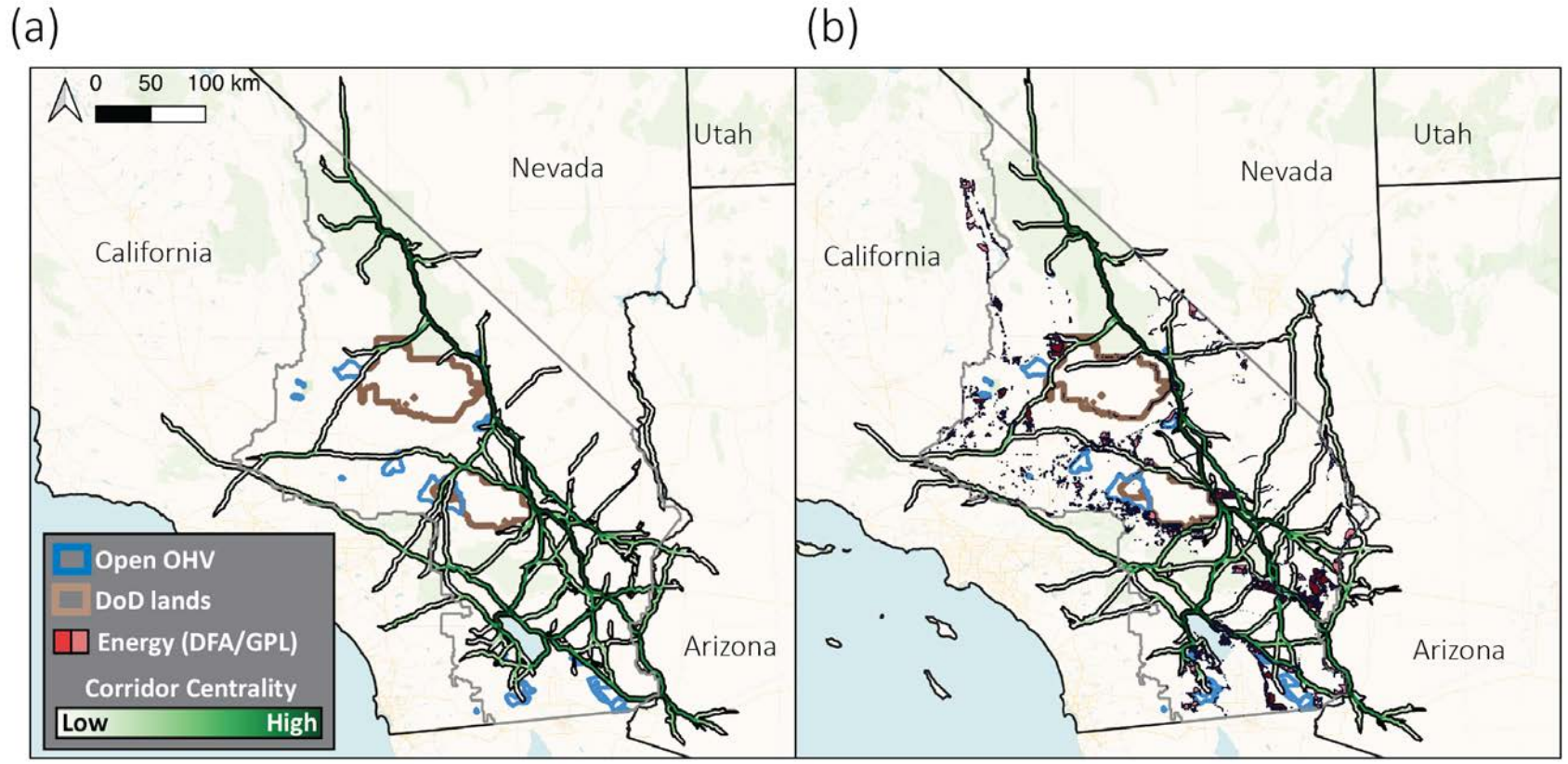

Figure 11. Map of predicted desert kit fox corridors under (a) the present day scenario with moderately permeable roads and railways (Scenario 2) and under (b) the high intensity future scenario (Scenario 4). Increasing corridor centrality (i.e., the number of random least cost paths overlapping a given corridor) is indicated by darker shades of green. Open off-highway vehicle (OHV) areas (blue polygons) and major Department of Defense (DoD) installations (brown polygons) are shown for reference. Areas authorized for solar energy development are shown in shades of red, with Development Focused Areas (DFA) and Variance Process Lands (VPL) shown as dark red polygons and General Public Lands (GPL) shown as pink polygons. Both scenarios also included OHV trail density, but trails are excluded here for clarity.

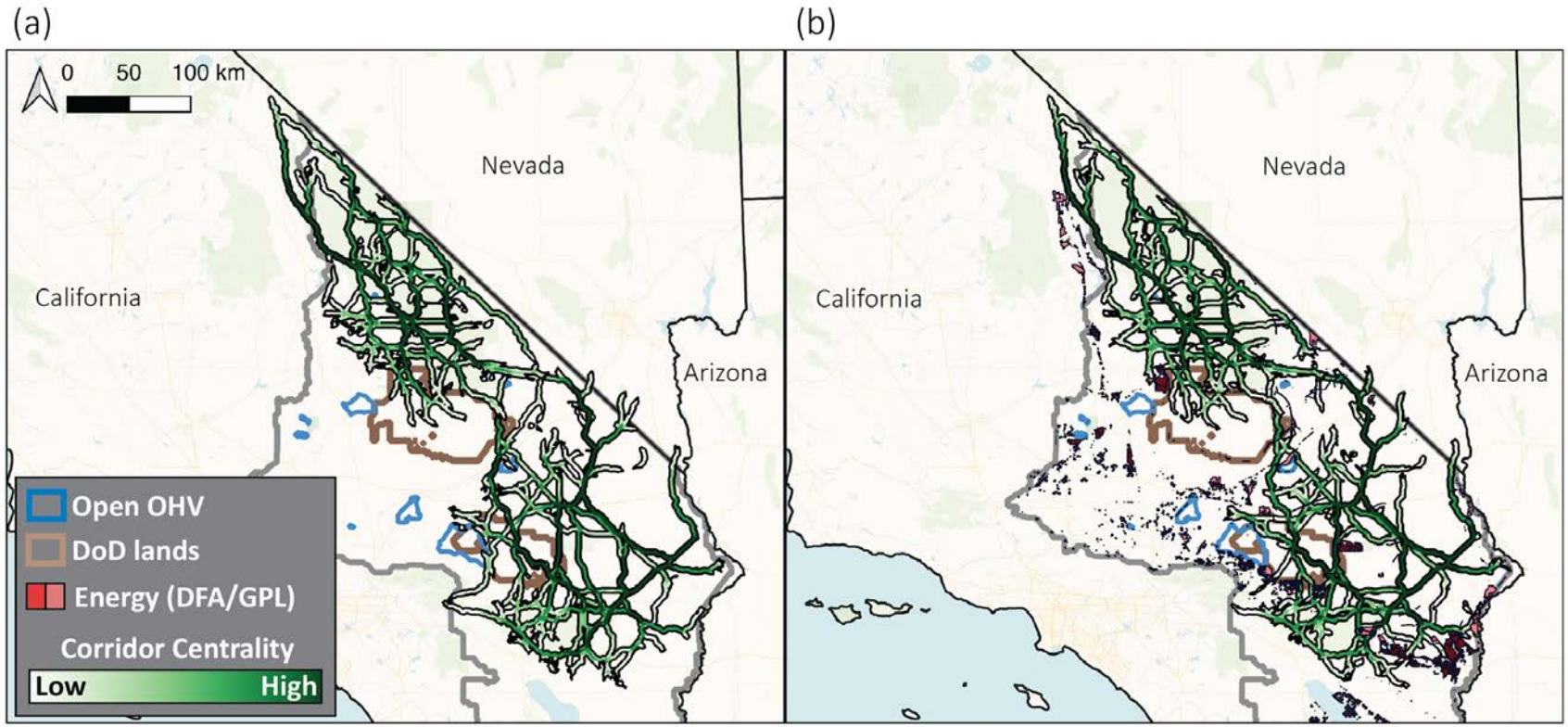

Figure 12. Map of predicted desert bighorn sheep corridors under (a) the present day scenario with moderately permeable roads and railways (Scenario 2) and under (b) the high intensity future scenario (Scenario 4). Corridors were derived separately for the two bighorn populations considered here (i.e., the Mojave Desert population in the south and the Death Valley population in the north) and overlaid on this map. Increasing corridor centrality (i.e., the number of random least cost paths overlapping a given corridor) is indicated by darker shades of green. Open off-highway vehicle (OHV) areas (blue polygons) and major Department of Defense (DoD) installations (brown polygons) are shown for reference. Areas authorized for solar energy development are shown in shades of red, with Development Focused Areas (DFA) and Variance Process Lands (VPL) shown as dark red polygons and General Public Lands (GPL) shown as pink polygons. Both scenarios also included OHV trail density, but trails are excluded here for clarity.

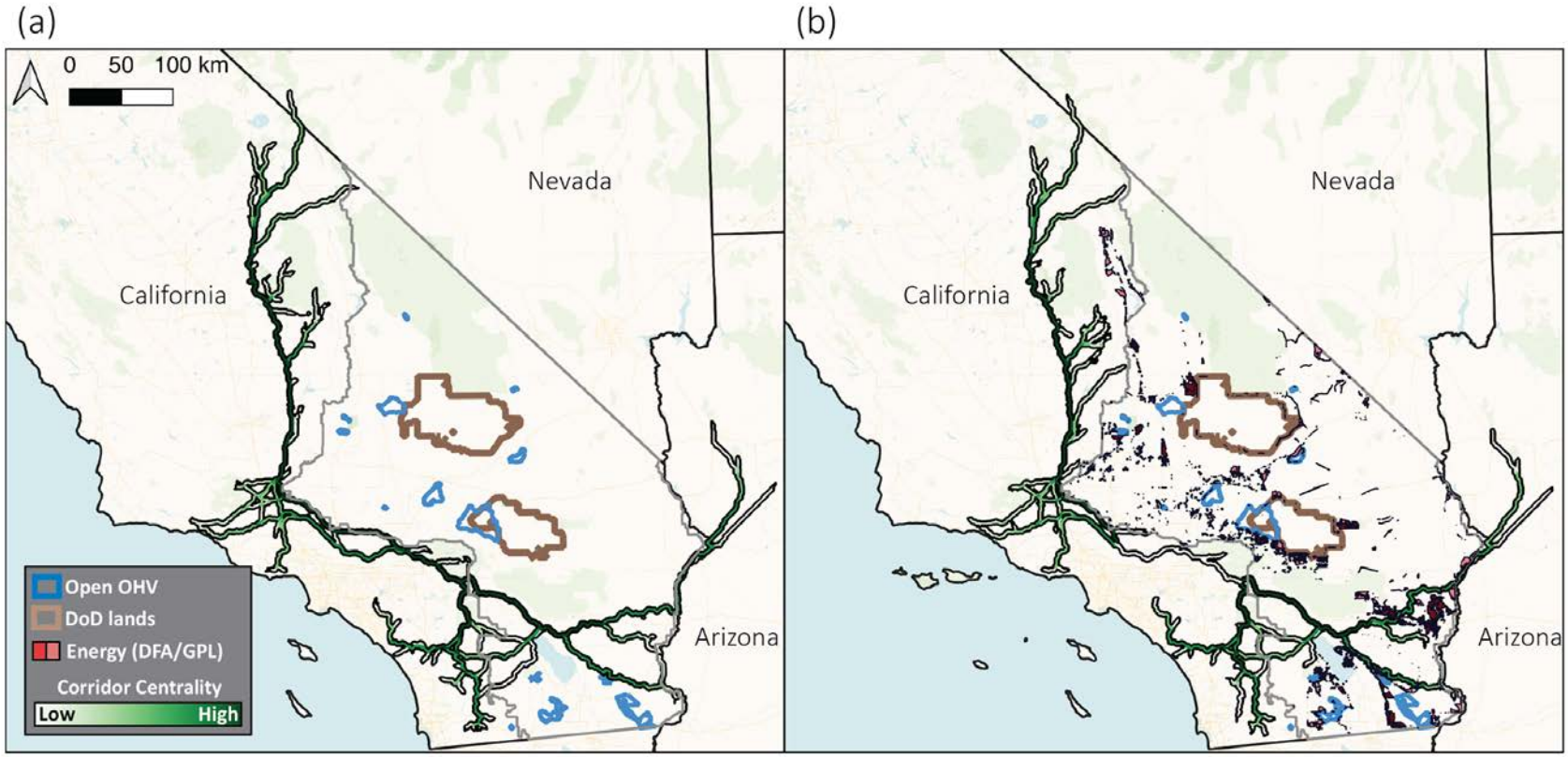

Figure 13. Map of predicted mule deer corridors under (a) the present day scenario with moderately permeable roads and railways (Scenario 2) and under (b) the high intensity future scenario (Scenario 4). Increasing corridor centrality (i.e., the number of random least cost paths overlapping a given corridor) is indicated by darker shades of green. Open off-highway vehicle (OHV) areas (blue polygons) and major Department of Defense (DoD) installations (brown polygons) are shown for reference. Areas authorized for solar energy development are shown in shades of red, with Development Focused Areas (DFA) and Variance Process Lands (VPL) shown as dark red polygons and General Public Lands (GPL) shown as pink polygons. Both scenarios also included OHV trail density, but trails are excluded here for clarity.

3.2 Multispecies corridors

Multispecies corridors for each scenario are shown in Figures 14-21. When interpreting the multispecies corridor centrality maps (Figs. 14, 16, 18, and 20), it is important to note that a corridor with high multispecies centrality means that, regardless of the number of species predicted to use a section of the corridor network, there was a high number of overlapping random least cost paths through that area. Thus, as described in Section 2.5 above, high centrality in these corridors does not necessarily correspond to a high conservation value for multiple species but could instead indicate particularly high importance for a single species (e.g., the high-centrality north-south corridor through the mountains along the western edge of the study area, driven largely by importance to MD). Centrality maps for each scenario should be viewed in combination with the corresponding species overlap map (Figs. 15, 17, 19, and 21), which present the total number of focal species predicted to use each segment of the multispecies corridor network.

Across scenarios, central portions of the study area (e.g., between the two major DoD installations) tended to have relatively high importance in terms of both corridor centrality and the number of focal species predicted to use these corridors. The importance of these areas only increases under the two future development scenarios (Figs. 18-21) as more peripheral regions of the study area are exposed to increasing solar development. This may lead to reduced path redundancy, and a greater relative importance of the most central corridors for maintaining landscape connectivity. As a consequence, maintaining these central corridors becomes more critical for maintaining the integrity and connectedness of the broader corridor network and landscape as a whole. Our analysis also highlights the importance of DoD lands in supporting multispecies connectivity in the CDCA. Across scenarios, several high-centrality and high-species overlap corridors were predicted to pass through portions of the two major DoD installations with relatively low maneuver intensity, suggesting that military partners will be important collaborators in managing for the persistence of wildlife habitat in the region.

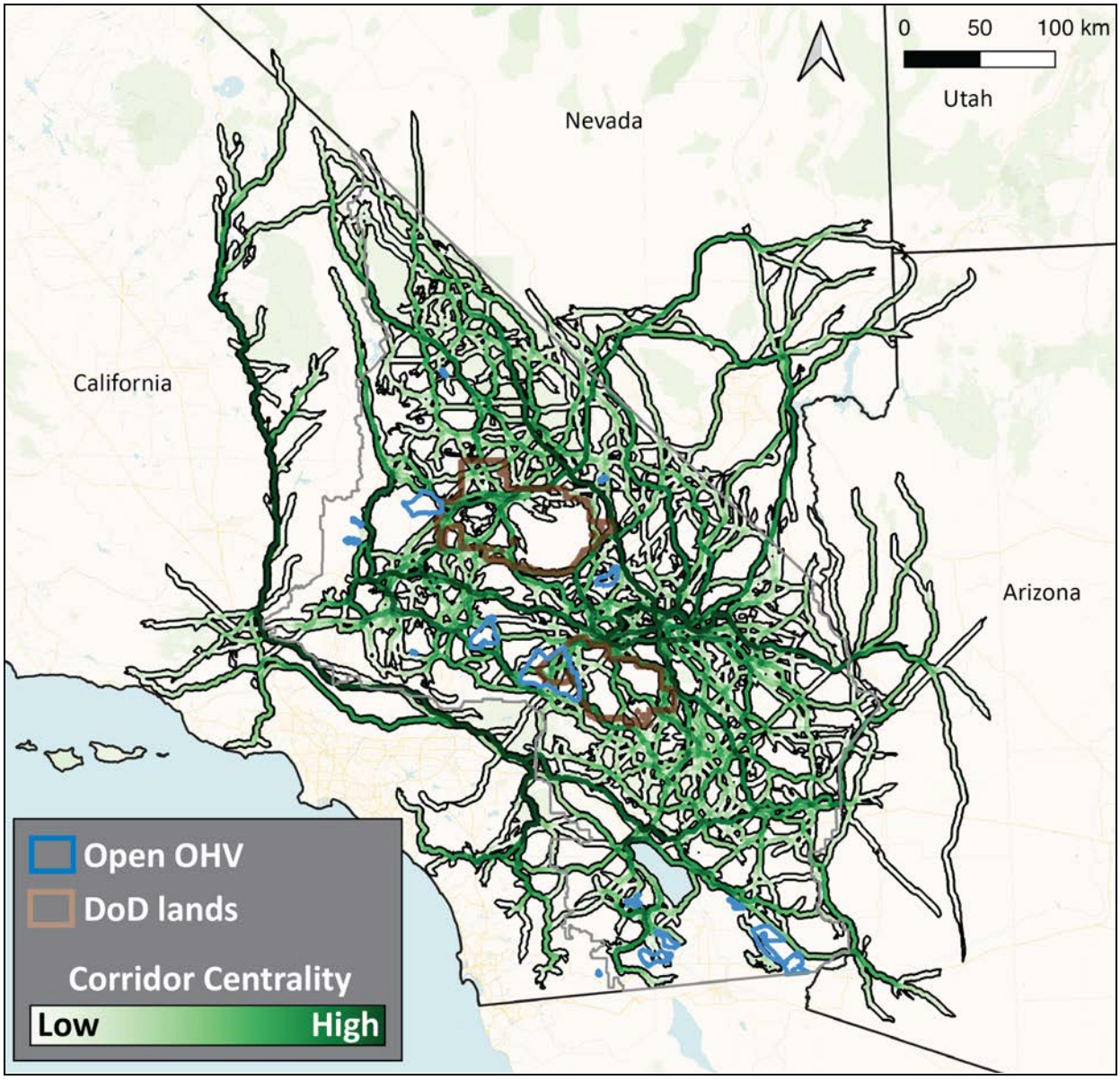

Figure 14. Map of multispecies corridor centrality for the present day scenario with minimally permeable roads and railways (Scenario 1). Increasing corridor centrality (i.e., the number of random least cost paths overlapping a given corridor across all focal species) is indicated by darker shades of green. Open off-highway vehicle (OHV) areas (blue polygons) and major Department of Defense (DoD) installations (brown polygons) are shown for reference. This scenario also included OHV trail density, but trails are excluded here for clarity.

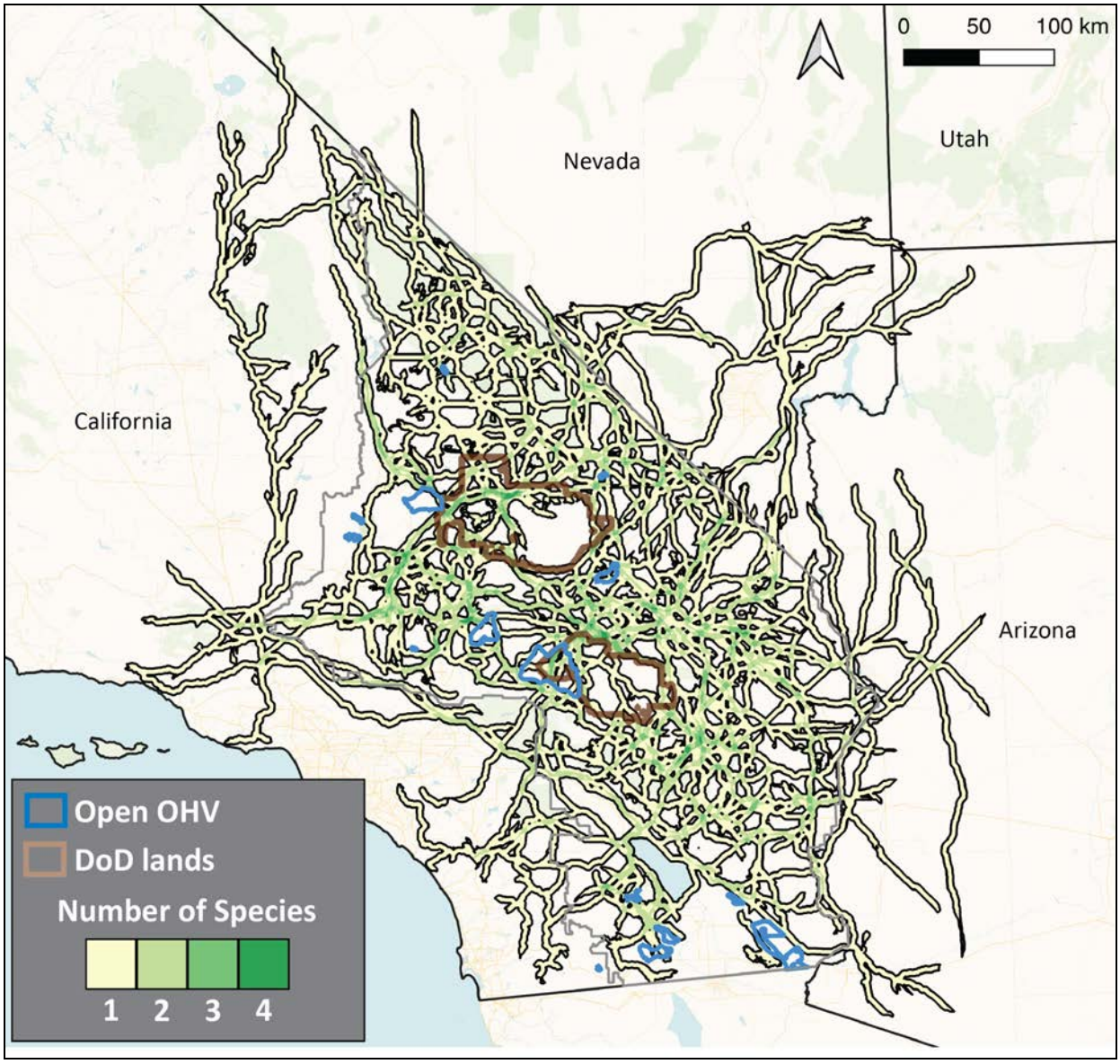

Figure 15. Map of focal species overlap in the multispecies corridor network for the present day scenario with minimally permeable roads and railways (Scenario 1). Open off-highway vehicle (OHV) areas (blue polygons) and major Department of Defense (DoD) installations (brown polygons) are shown for reference. This scenario also included OHV trail density, but trails are excluded here for clarity.

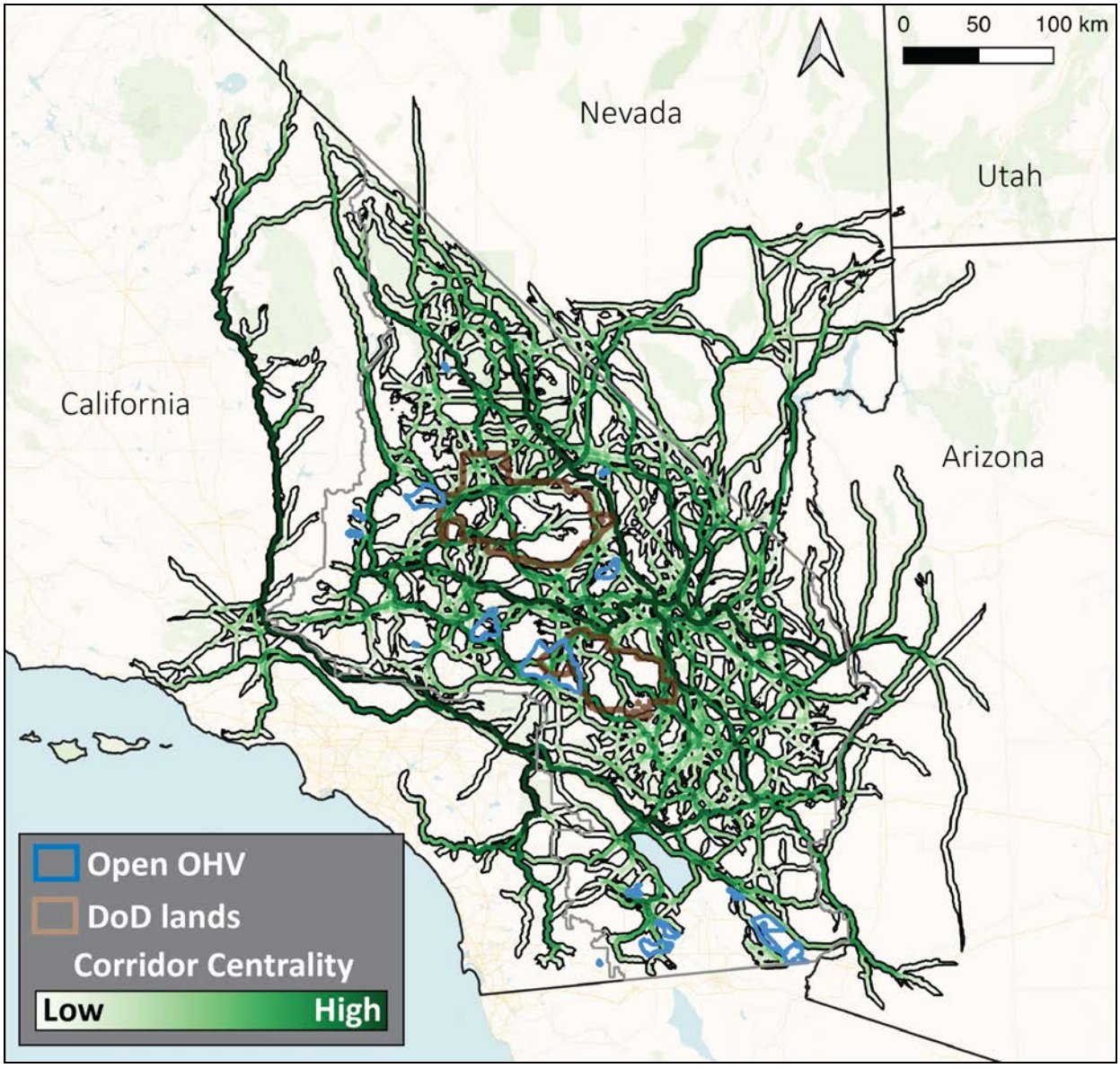

Figure 16. Map of multispecies corridor centrality for the present day scenario with moderately permeable roads and railways (Scenario 2). Increasing corridor centrality (i.e., the number of random least cost paths overlapping a given corridor across all focal species) is indicated by darker shades of green. Open off-highway vehicle (OHV) areas (blue polygons) and major Department of Defense (DoD) installations (brown polygons) are shown for reference. This scenario also included OHV trail density, but trails are excluded here for clarity.

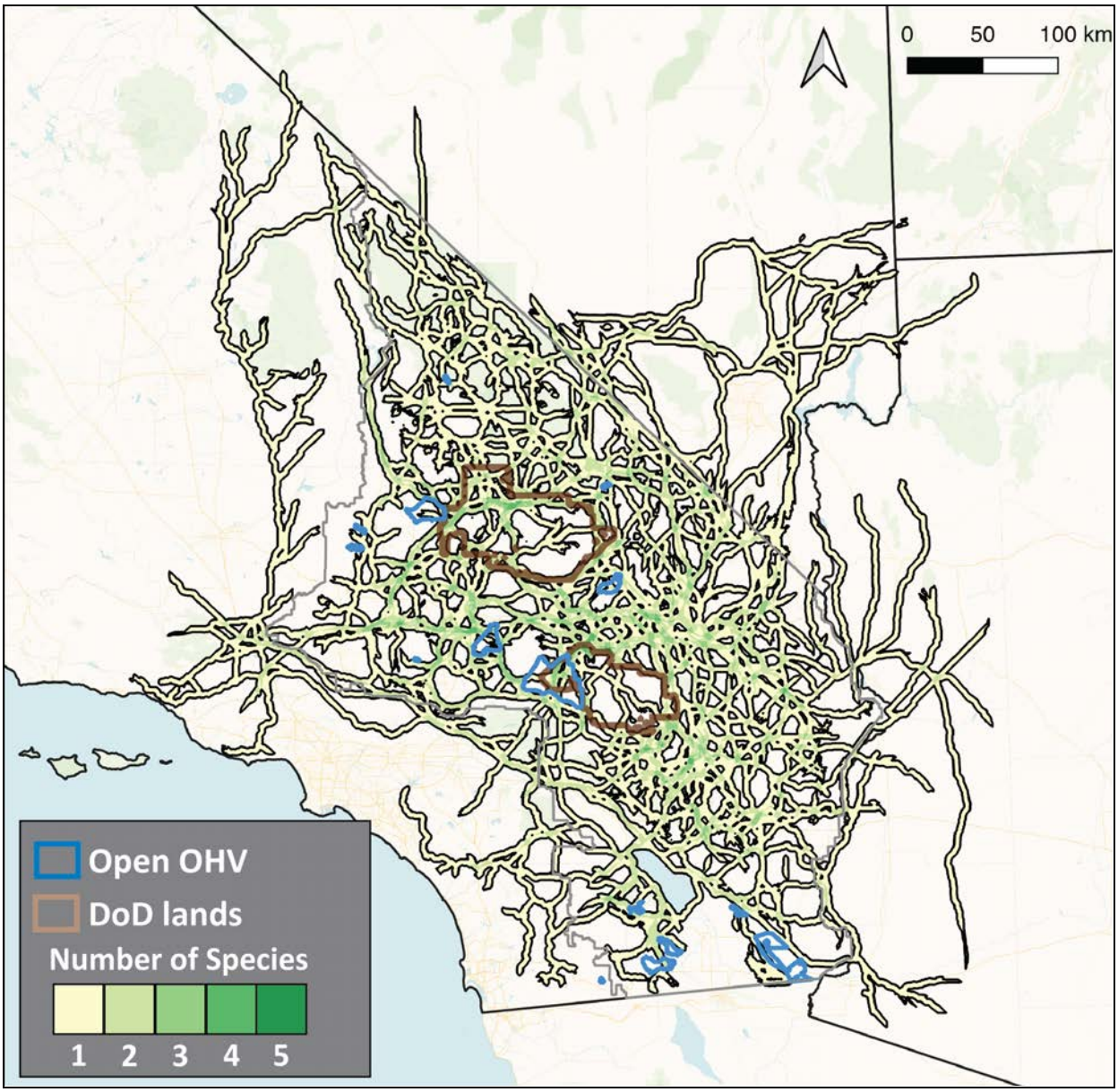

Figure 17. Map of focal species overlap in the multispecies corridor network for the present day scenario with moderately permeable roads and railways (Scenario 2). Open off-highway vehicle (OHV) areas (blue polygons) and major Department of Defense (DoD) installations (brown polygons) are shown for reference. This scenario also included OHV trail density, but trails are excluded here for clarity.

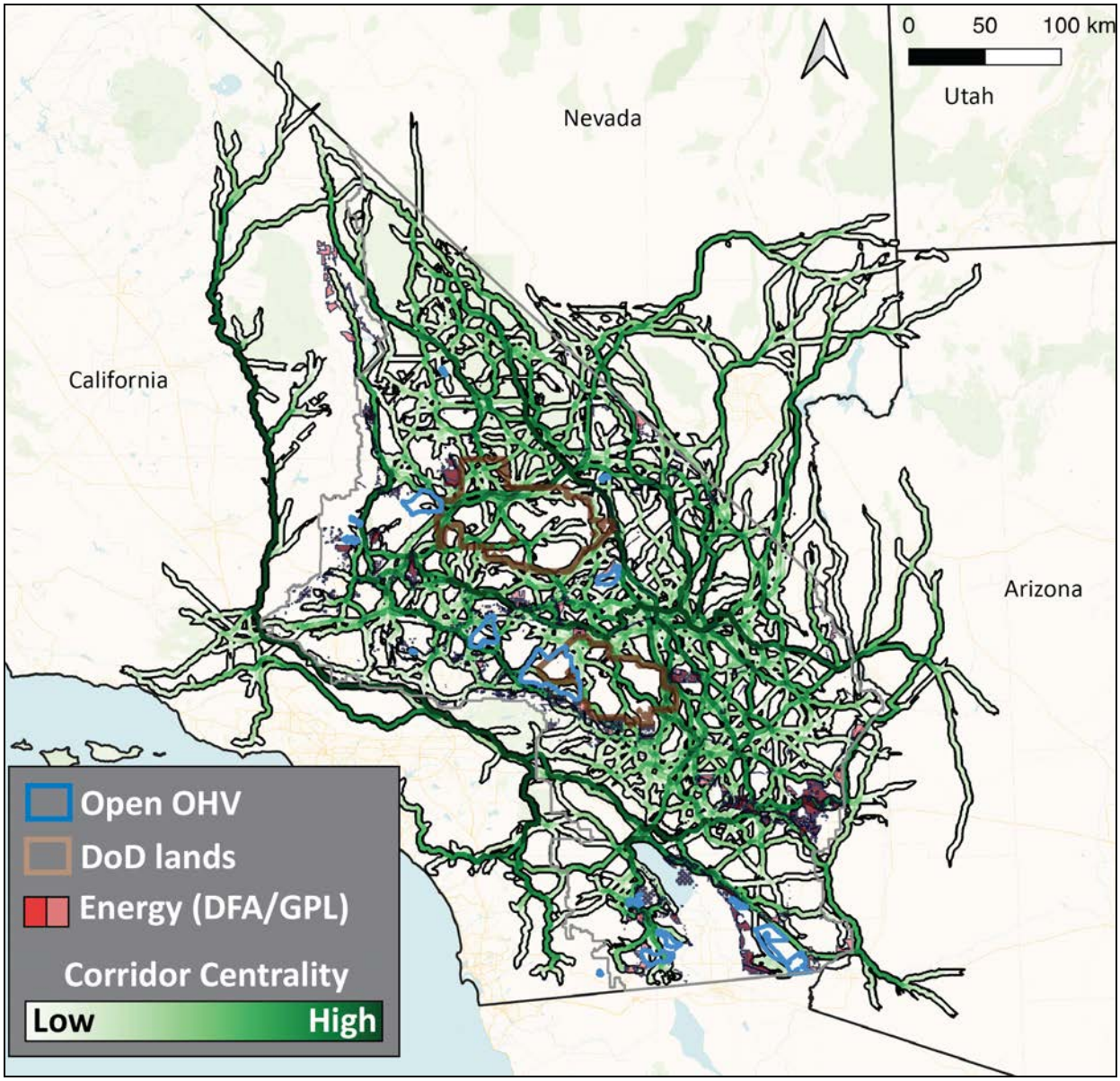

Figure 18. Map of multispecies corridor centrality under the moderate intensity future scenario (Scenario 3). Increasing corridor centrality (i.e., the number of random least cost paths overlapping a given corridor across all focal species) is indicated by darker shades of green. Open off-highway vehicle (OHV) areas (blue polygons) and major Department of Defense (DoD) installations (brown polygons) are shown for reference. Areas authorized for solar energy development are shown in shades of red, with Development Focused Areas (DFA) and Variance Process Lands (VPL) shown as dark red polygons and General Public Lands (GPL) shown as pink polygons. This scenario also included OHV trail density, but trails are excluded here for clarity.

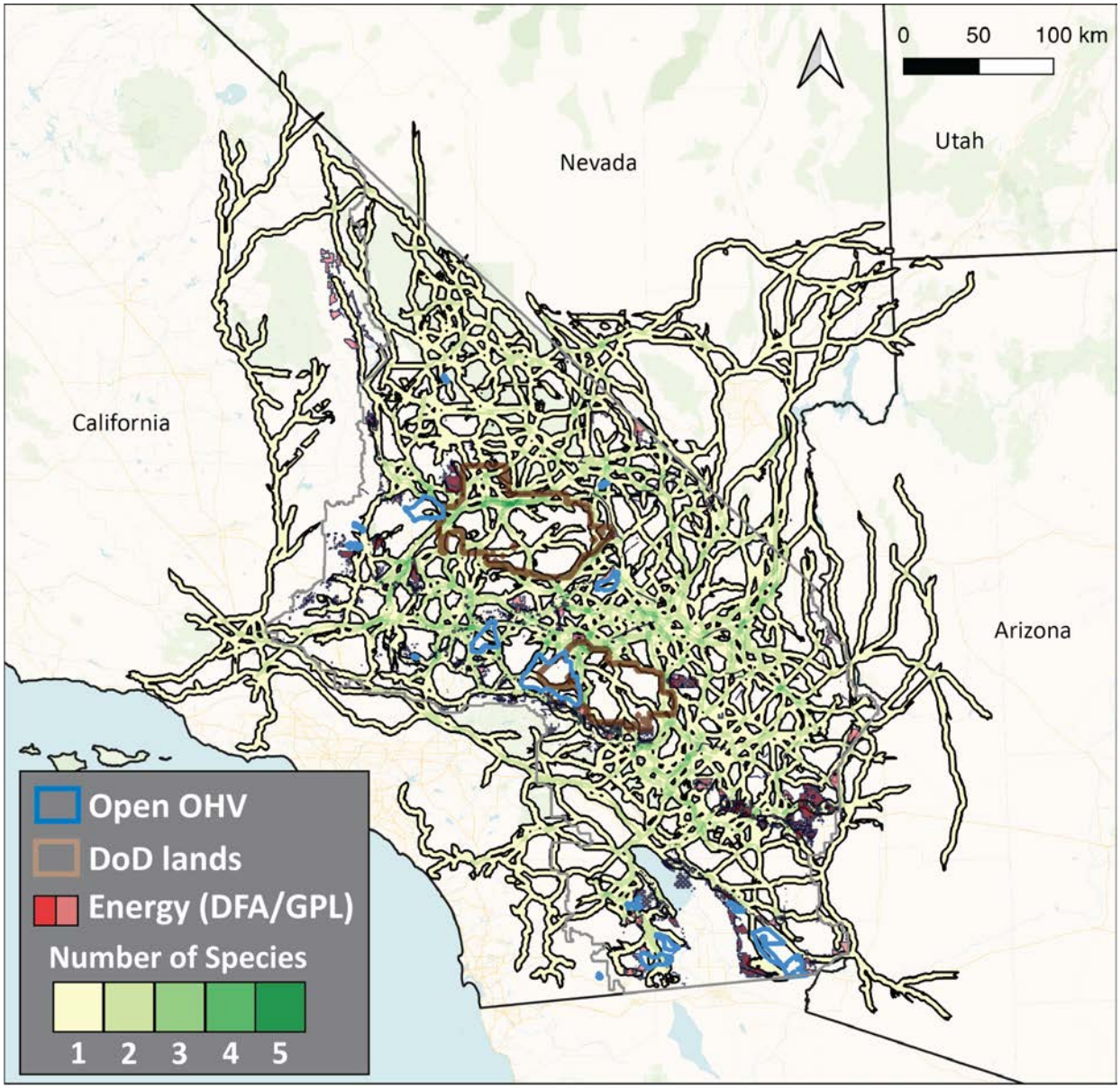

Figure 19. Map of focal species overlap under the moderate intensity future scenario (Scenario 3). Open off-highway vehicle (OHV) areas (blue polygons) and major Department of Defense (DoD) installations (brown polygons) are shown for reference. Areas authorized for solar energy development are shown in shades of red, with Development Focused Areas (DFA) and Variance Process Lands (VPL) shown as dark red polygons and General Public Lands (GPL) shown as pink polygons. This scenario also included OHV trail density, but trails are excluded here for clarity.

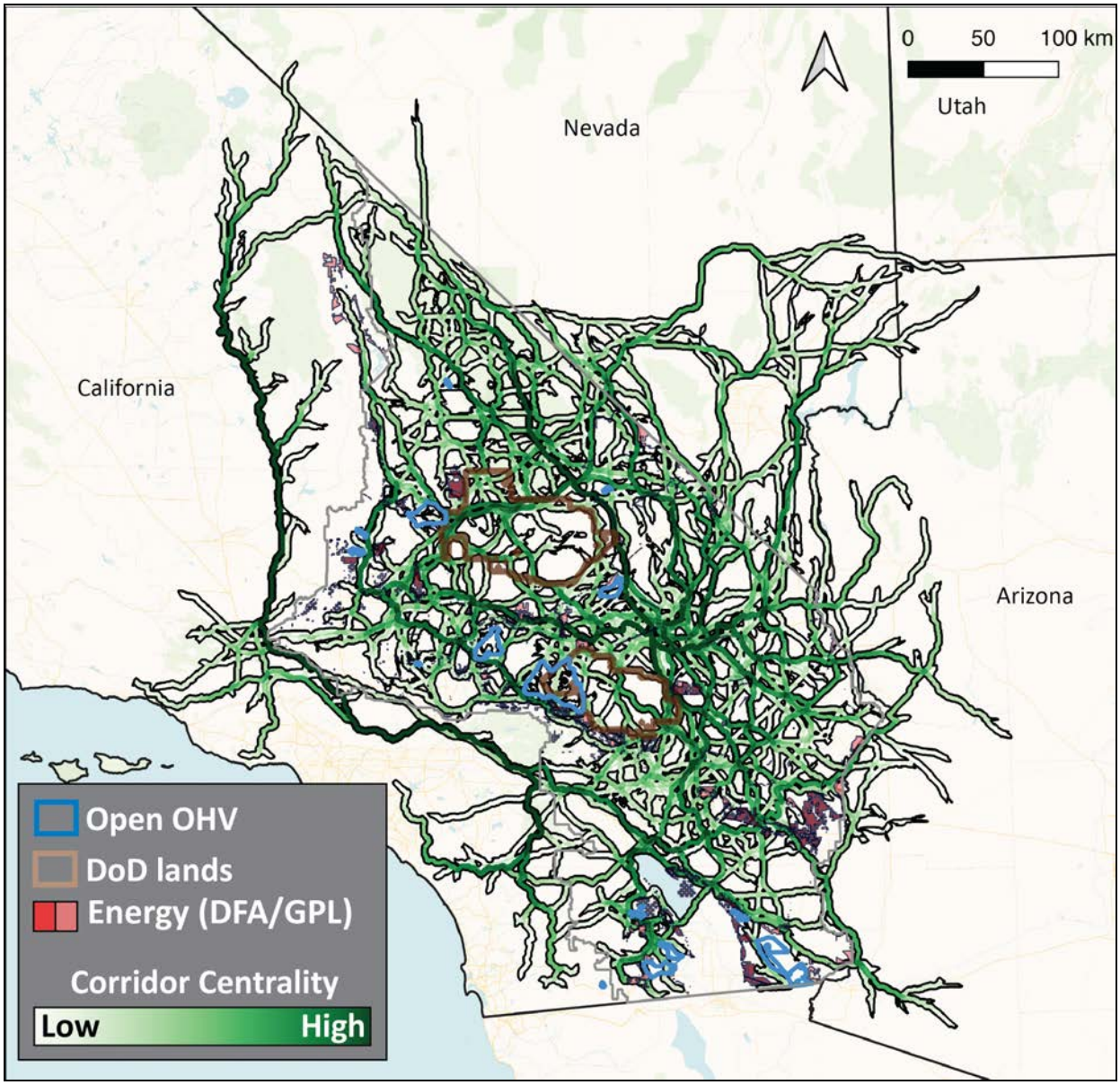

Figure 20. Map of multispecies corridor centrality under the high-intensity future scenario (Scenario 4). Increasing corridor centrality (i.e., the number of random least cost paths overlapping a given corridor across all focal species) is indicated by darker shades of green. Open off-highway vehicle (OHV) areas (blue polygons) and major Department of Defense (DoD) installations (brown polygons) are shown for reference. Areas authorized for solar energy development are shown in shades of red, with Development Focused Areas (DFA) and Variance Process Lands (VPL) shown as dark red polygons and General Public Lands (GPL) shown as pink polygons. This scenario also included OHV trail density, but trails are excluded here for clarity.

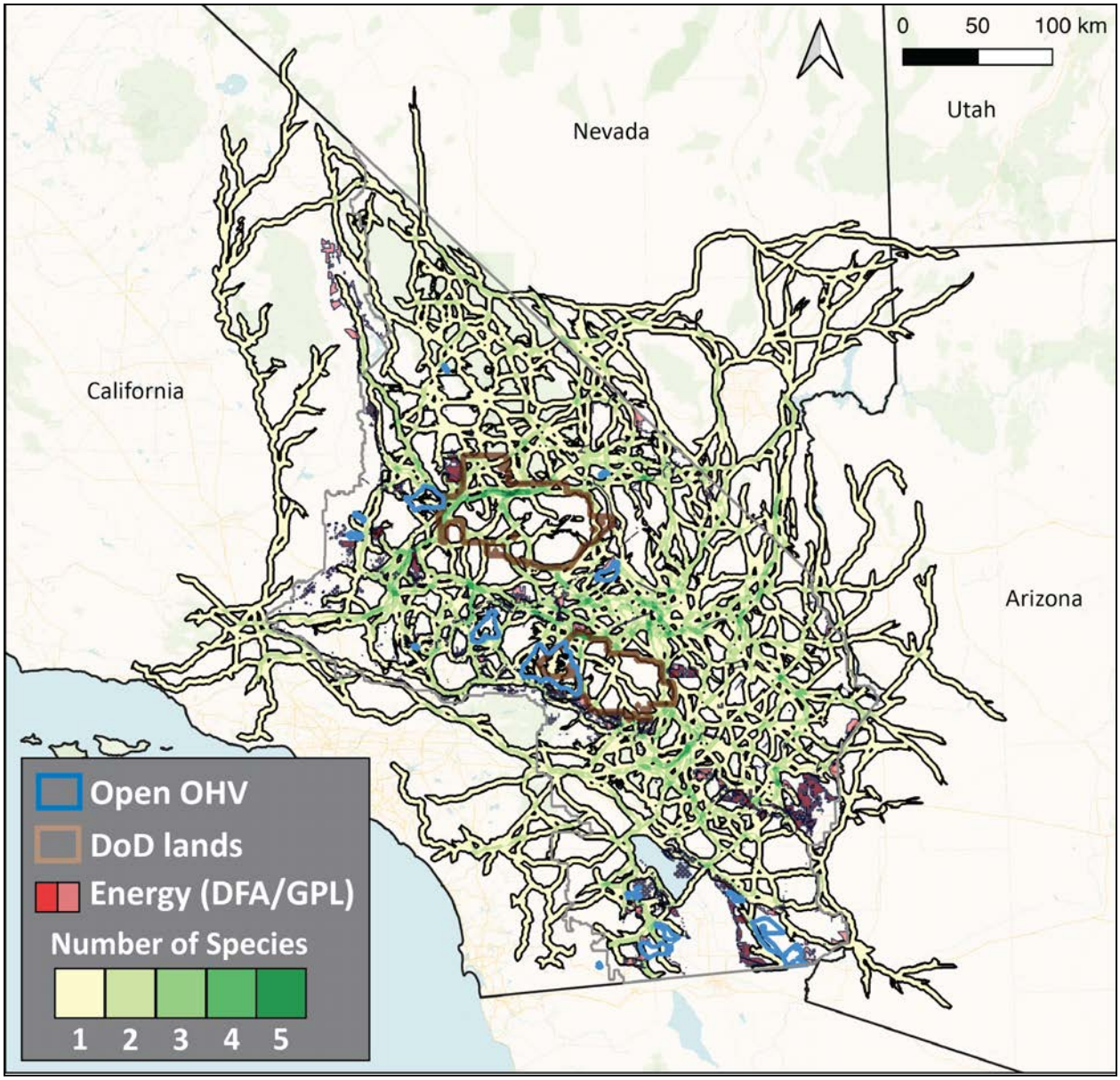

Figure 21. Map of focal species overlap under the high-intensity future scenario (Scenario 4). Open off-highway vehicle (OHV) areas (blue polygons) and major Department of Defense (DoD) installations (brown polygons) are shown for reference. Areas authorized for solar energy development are shown in shades of red, with Development Focused Areas (DFA) and Variance Process Lands (VPL) shown as dark red polygons and General Public Lands (GPL) shown as pink polygons. This scenario also included OHV trail density, but trails are excluded here for clarity.

3.3 Parcelization of multispecies corridors

The degree to which the land comprising a high-value wildlife corridor is divided into privately held parcels may substantially influence management of that corridor. Corridors overlaying a large number of private parcels may be considerably more difficult to manage than those overlaying fewer private parcels or publicly managed lands given the potentially large number of private landowners a manager would need to engage to protect a heavily parcelized corridor. Figures 22 through 25 display the results of our parcelization analysis quantifying the degree of parcelization (and thus potential manageability) of multispecies corridors across the CDCA. For each scenario, we present private parcel density (number of distinct private parcels per unit area) for each multispecies corridor segment falling with the CDCA boundary and compare this the number of species predicted to use that segment (see left and right panels in Figs. 22 to 25), allowing a visual approximation of where particularly high-value corridor segments overlap with heavily parcelized private land.

The large majority of private lands in the CDCA (and thus the most heavily parcelized corridors) occur in the western and southern portions of the study area. The area west of Highway 395 contains a large concentration of corridors with relatively high species overlap falling on largely private lands. Outside of the city of Lancaster, this area of the CDCA is currently only moderately developed (and is therefore predicted by our models to support substantial wildlife movement). However, this area may represent a considerable management challenge given the substantial amounts of small-to-moderately sized private parcels that could potentially be developed for suburban housing or utility scale solar. This is similarly the case for high connectivity private lands to the north and west of the Salton Sea. By contrast, private land is somewhat sparser in the central and eastern portions of the CDCA, which may imply greater manageability of high-value corridors in these regions where private parcel density within corridors tends to be lower. For this analysis, we also calculated the total number of parcels and average parcel area within each corridor segment. These values are provided as part of the datasets associated with this report.

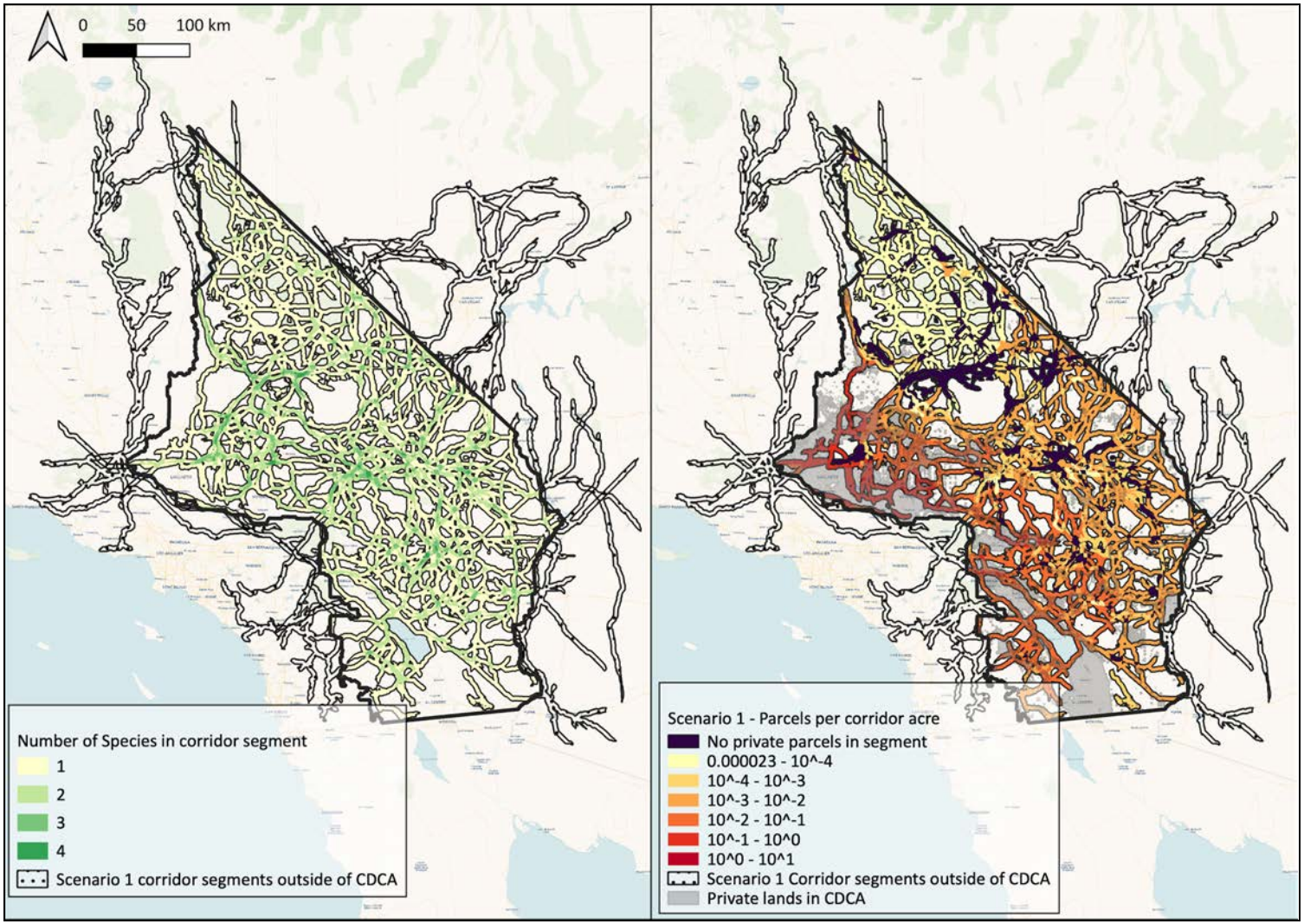

Figure 22. Maps showing the overlap of focal species corridors within the CDCA (left) and private parcel density (right; calculated as the number of private parcels per acre of corridor segment within the CDCA boundary) under the present-day scenario with minimally permeable roads and railways (Scenario 1). Parcel densities are presented on a logarithmic scale. Analysis of parcel density was constrained to the area inside the CDCA boundary only. Corridor segments that did not contain any private parcels are indicated in dark purple. Private lands are shown in gray.

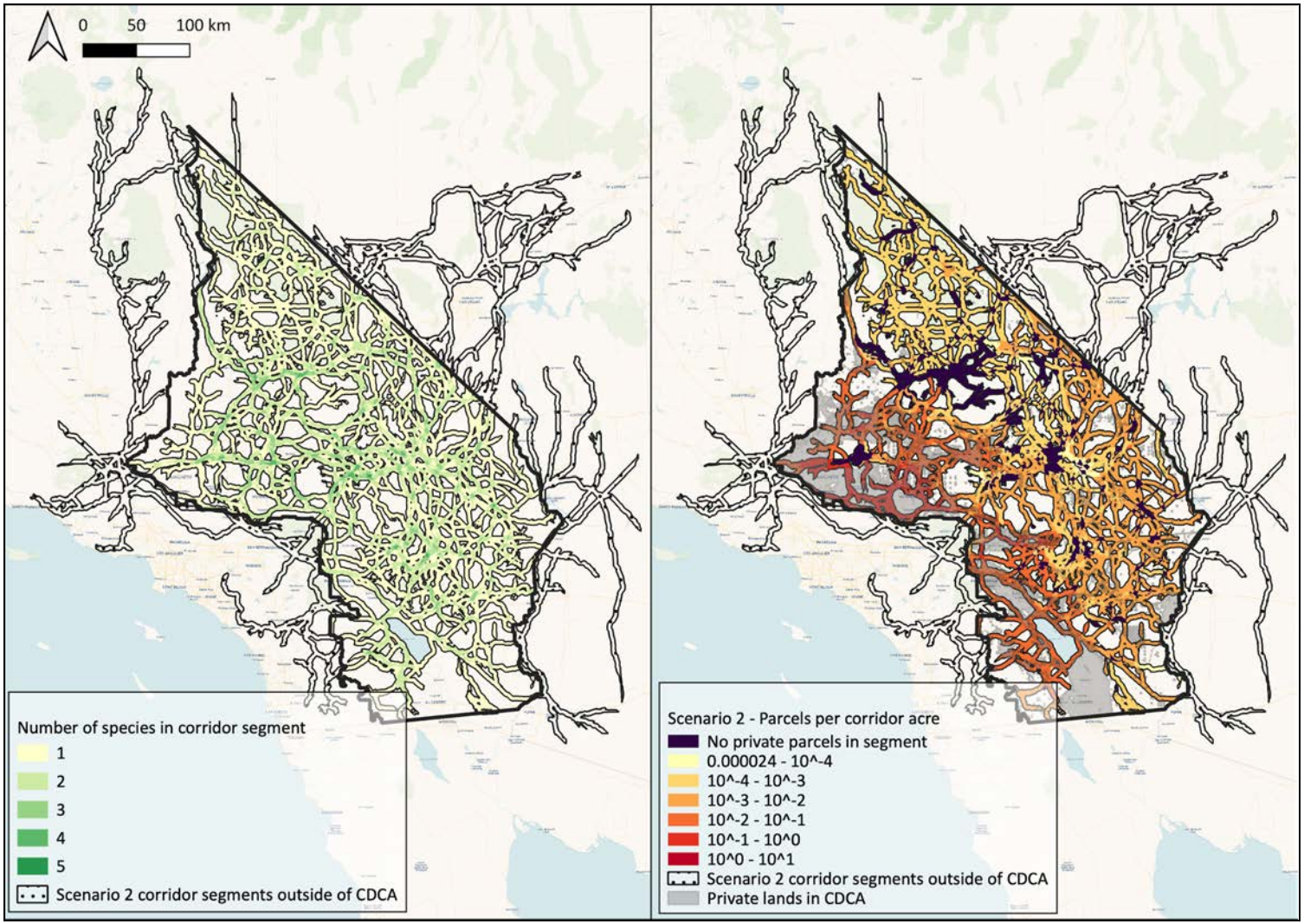

Figure 23. Maps showing the overlap of focal species corridors within the CDCA (left) and private parcel density (right; calculated as the number of private parcels per acre of corridor segment within the CDCA boundary) under the present-day scenario with moderately permeable roads and railways (Scenario 2). Parcel densities are presented on a logarithmic scale. Analysis of parcel density was constrained to the area inside the CDCA boundary only. Corridor segments that did not contain any private parcels are indicated in dark purple. Private lands are shown in gray.

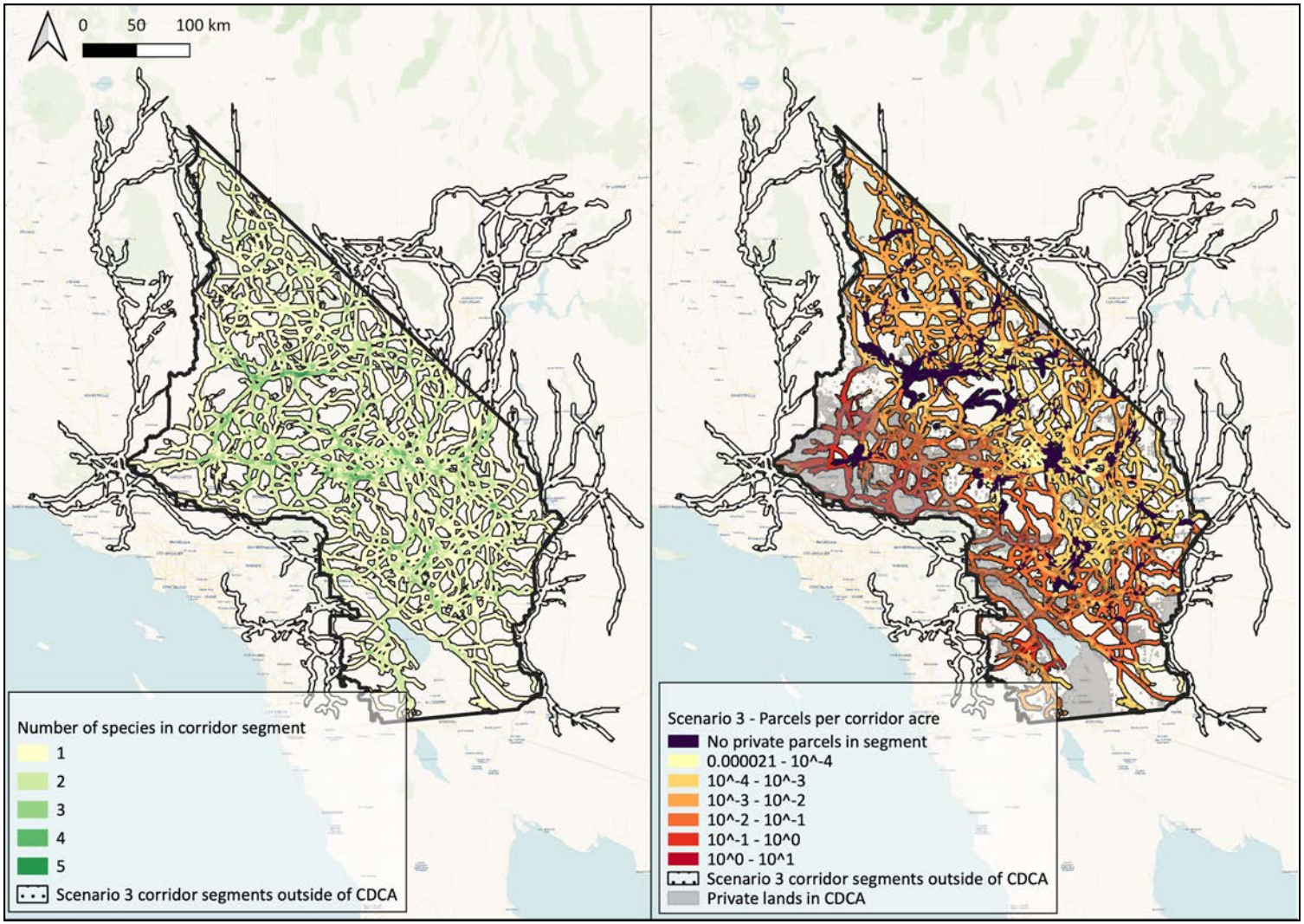

Figure 24. Maps showing the overlap of focal species corridors within the CDCA (left) and private parcel density (right; calculated as the number of private parcels per acre of corridor segment within the CDCA boundary) under the moderate intensity future scenario (Scenario 3). Parcel densities are presented on a logarithmic scale. Analysis of parcel density was constrained to the area inside the CDCA boundary only. Corridor segments that did not contain any private parcels are indicated in dark purple. Private lands are shown in gray.

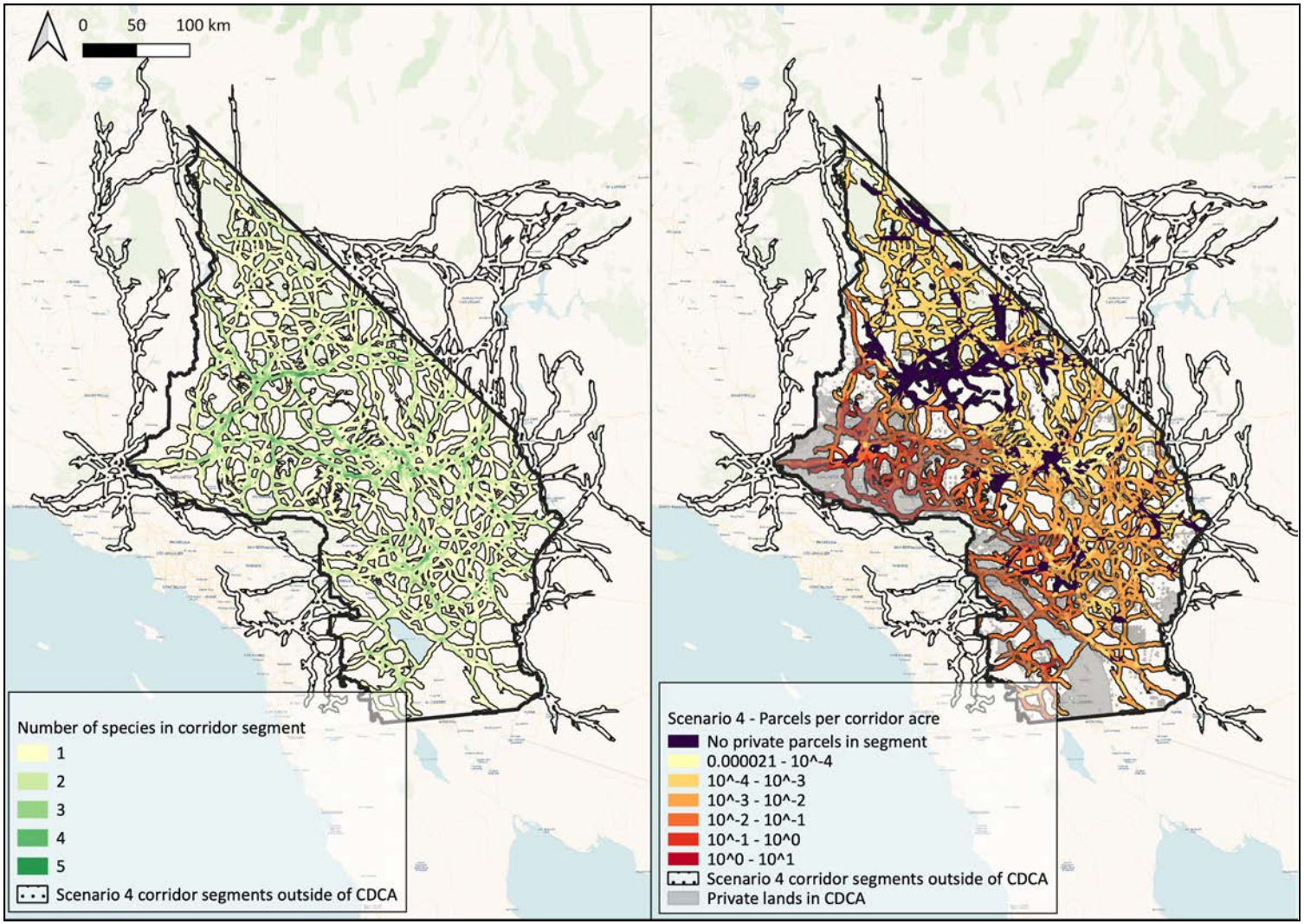

Figure 25. Maps showing the overlap of focal species corridors within the CDCA (left) and private parcel density (right; calculated as the number of private parcels per acre of corridor segment within the CDCA boundary) under the high intensity future scenario (Scenario 4). Parcel densities are presented on a logarithmic scale. Analysis of parcel density was constrained to the area inside the CDCA boundary only. Corridor segments that did not contain any private parcels are indicated in dark purple. Private lands are shown in gray.

4. DATA USES AND LIMITATIONS

The analyses presented here, including all single-species models and the multispecies corridor maps, reflect a regional-scale evaluation of wildlife movement pathways in the CDCA. The primary goal of the analysis was to identify general areas across the CDCA that are likely to provide valuable connectivity corridors as opposed to predicting fine-scale wildlife movement throughout the study area. Results should be interpreted with this in mind, and connectivity maps and predicted wildlife corridors should be used to target further on-the-ground investigation to confirm the locations of high-value movement habitat for the focal species.

Given the relatively large size of the study area (the CDCA is approximately 105,000 km^2) and the number of focal species for which connectivity was modeled, we took a regional-scale approach, focusing on general predictors of habitat quality (e.g., topography, vegetation cover, climatic conditions) and landscape resistance (e.g., major roads and developments) to derive estimates of wildlife movement potential across this large area. As such, this analysis may overlook some localized landscape features (e.g., specific vegetation types, prey availability) that could influence wildlife habitat suitability and movement. We also focused our analyses on potential connectivity, i.e., whether the landscape is likely to support movement by a species based on the underlying habitat suitability and intensity of human land use. In some cases, areas predicted to support movement may differ from those known to be heavily used by the species in question. This approach was adopted to allow consideration of areas that may prove valuable for species connectivity if conservation/mitigation measures are taken.

Our regional approach to defining species corridors and ranking corridors based on centrality prioritizes maintaining connectivity across the entire network of potential movement pathways and does not necessarily capture all areas of high animal movement. Thus, the absence of a corridor in a given location does not imply that the location is unsuitable for wildlife movement or that it should be ignored when making conservation decisions. Rather, the absence of a corridor simply means that movement through that location is predicted to be less central to the overall connectivity of the corridor network. For instance, places at the periphery of the study area are, by definition, not central to the entire corridor network and may therefore have no or only low-ranking corridors identified despite such peripheral areas often being important for species conservation (Channell and Lomolino 2000). Relatedly, corridors with high centrality are predicted to be highly important in maintaining connectivity across the entire study area, but do not necessarily align with the areas of highest wildlife movement. We therefore recommend that focal species corridors and current flow maps be interpreted together. Users can view the corridor map to locate key movement pathways for maintaining network connectivity and use the current flow map, which estimates the predicted likelihood of animal movement through each pixel on the landscape, to determine the locations that are likely to experience the highest intensity of movement for a given species. It is also important to note that corridors in our analysis were given an arbitrarily large width (4 km), and thus corridor width in itself does not provide information on the best movement habitat within the corridor. Here again we encourage users to view the current flow map to identify the areas of highest predicted movement potential within a given corridor when determining where to focus on-the-ground conservation efforts.

Our use of habitat suitability surfaces in generating connectivity models may have resulted in corridor locations that largely reflect areas of habitat suitable for home range use. However, research indicates that many wildlife species are willing to move through lower quality habitat when dispersing, relative to the quality of habitat needed for home range selection (Elliot et al. 2014, Abrahms et al. 2017). High temporal resolution movement data, which is required to differentiate dispersal movements from other activities, were largely unavailable for the species and study area addressed here, necessitating our reliance on coarser resolution location or count data and species distribution models. Thus our analysis may omit some pathways through relatively low quality areas that could be used by dispersing animals, but likely captures the majority of important, frequently used movement pathways. Relatedly, rugged areas may be underrepresented as potential movement habitat in our predicted corridors for MDT. Our data inputs for MDT connectivity models, representing the most contemporary rangewide estimates of tortoise habitat quality and movement habitat suitability (see Section 2.3 above), identified rugged terrain as relatively unsuitable for tortoises due to a lack of tortoise location data in rugged areas. However, recent work has suggested that moderately rugged terrain may support MDT in terms of home range and movement habitat selection (Dutcher et al. 2020, Hromada et al. 2020).

Finally, it is important to note that the predictions and maps generated in this analysis come with some level of uncertainty. As described in Section 2, our workflow began with predicting habitat suitability, followed by mapping resistance, running Omniscape models, and finally running least cost-path analyses. Each step involved some amount of uncertainty stemming from, e.g., measurement error in spatial inputs/covariates, covariate selection, methodological decision points, and model parameter selection (e.g., Omniscape settings for moving window radii and source strength thresholds). Further, error at earlier steps in the workflow is propagated to subsequent steps such that least cost paths (the final step in our workflow) are subject to uncertainty at all previous modeling stages. Any multi-step modeling process such as ours inherently involves compounding uncertainty, whether due to data quality and limitations or methodological decision points. Unfortunately, there are no methods available for reliably quantifying uncertainty from these disparate sources. Our results should be interpreted with these uncertainties in mind. We again note that the connectivity surfaces and corridors presented here are predictions of areas likely to be important for animal movement and, where feasible, should be validated using on-the-ground surveys of species presence and habitat use.

REFERENCES (including works cited in appendices)

Abrahms, B., S. C. Sawyer, N. R. Jordan, J. W. McNutt, A. M. Wilson, and J. S. Brashares. 2017. Does wildlife resource selection accurately inform corridor conservation? Journal of Applied Ecology 54:412–422.

Anantharaman, R., K. Hall, V. B. Shah, and A. Edelman. 2020. Circuitscape in Julia: High performance connectivity modelling to support conservation decisions. Proceedings of the JuliaCon Conferences 1:58.

Averill-Murray, R. C., C. R. Darst, N. Strout, and M. Wong. 2013. Conserving population linkages for the Mojave desert tortoise (Gopherus agassizii). Herpetological Conservation and Biology 8:15.

Bezanson, J., A. Edelman, S. Karpinski, and V. B. Shah. 2017. Julia: A Fresh Approach to Numerical

Computing. SIAM Review 59:65–98.
BLM. 2022. National Surface Management Agency Area Polygons - National Geospatial Data Asset (NGDA). Bureau of Land Management. https://www.arcgis.com/home/item.html?id=6bf2e737c59d4111be92420ee5ab0b46.
Boyce, M. S., P. R. Vernier, S. E. Nielsen, and F. K. A. Schmiegelow. 2002. Evaluating resource selection functions. Ecological Modelling 157:281–300.
Burnham, K. P., and D. R. Anderson. 2002. Model Selection and Multimodel Inference: A Practical Information-Theoretic Approach. Second edition. Springer, New York.
Cameron, D. R., B. S. Cohen, and S. A. Morrison. 2012. An approach to enhance the conservation-compatibility of solar energy development. PLOS ONE 7:e38437.
Channell, R., and M. V. Lomolino. 2000. Dynamic biogeography and conservation of endangered species. Nature 403:84–86.
Chen, H. L., and J. L. Koprowski. 2019. Can we use body size and road characteristics to anticipate barrier effects of roads in mammals? a meta-analysis. Hystrix, the Italian Journal of Mammalogy 30:1–7.
Chetkiewicz, C.-L. B., C. C. St. Clair, and M. S. Boyce. 2006. Corridors for conservation: Integrating pattern and process. Annual Review of Ecology, Evolution, and Systematics 37:317–342.
Conservation Science Partners. 2021. Modeling multi-species connectivity across the California Desert Conservation Area: A description of the approach, data, and analytical methods. Final Report. Truckee, CA.
Creech, T. G., C. W. Epps, E. L. Landguth, J. D. Wehausen, R. S. Crowhurst, B. Holton, and R. J. Monello. 2017. Simulating the spread of selection-driven genotypes using landscape resistance models for desert bighorn sheep. PLOS ONE 12:e0176960.
CSP. 2019. Methods and approach used to estimate the loss and fragmentation of natural lands in the conterminous U.S. from 2001 to 2017. Technical Report, Truckee, CA.
Dempsey, S. J., E. M. Gese, B. M. Kluever, R. C. Lonsinger, and L. P. Waits. 2015. Evaluation of scat deposition transects versus radio telemetry for developing a species distribution model for a rare desert carnivore, the kit fox. PLOS ONE 10:e0138995.
Denneboom, D., A. Bar-Massada, and A. Shwartz. 2021. Factors affecting usage of crossing structures by wildlife – A systematic review and meta-analysis. Science of The Total Environment 777:146061.
Dewitz, J. 2019. National Land Cover Database (NLCD) 2016 Products: U.S. Geological Survey data release.
Dewitz, J., and U.S. Geological Survey. 2021. National Land Cover Database (NLCD) 2019 Products (ver. 2.0, June 2021): U.S. Geological Survey data release. https://doi.org/10.5066/P9KZCM54.
Dickson, B. G., C. M. Albano, B. H. McRae, J. J. Anderson, D. M. Theobald, L. J. Zachmann, T. D. Sisk, and M. P. Dombeck. 2017. Informing strategic efforts to expand and connect protected areas using a model of ecological flow, with application to the western United States. Conservation Letters 10:564–571.
Dunnett, S., A. Sorichetta, G. Taylor, and F. Eigenbrod. 2020. Harmonised global datasets of wind and solar farm locations and power. Scientific Data 7:130.
Dutcher, K. E., A. G. Vandergast, T. C. Esque, A. Mitelberg, M. D. Matocq, J. S. Heaton, and K. E. Nussear. 2020. Genes in space: what Mojave desert tortoise genetics can tell us about landscape connectivity. Conservation Genetics 21:289–303.

Elliot, N. B., S. A. Cushman, D. W. Macdonald, and A. J. Loveridge. 2014. The devil is in the dispersers: predictions of landscape connectivity change with demography. Journal of Applied Ecology 51:1169–1178.

Epps, C. W., P. J. Palsbøll, J. D. Wehausen, G. K. Roderick, R. R. Ramey, and D. R. McCullough. 2005. Highways block gene flow and cause a rapid decline in genetic diversity of desert bighorn sheep. Ecology Letters 8:1029–1038.

Epps, C. W., J. D. Wehausen, V. C. Bleich, S. G. Torres, and J. S. Brashares. 2007. Optimizing dispersal and corridor models using landscape genetics. Journal of Applied Ecology 44:714–724.

Federal Railroad Administration. 2016. National Geospatial Data Asset (NGDA) North American Rail Lines. Office of the Assistant Secretary for Research and Technology/Bureau of Transportation Statistics, Washington, D.C.

Fletcher, R. J., N. S. Burrell, B. E. Reichert, D. Vasudev, and J. D. Austin. 2016. Divergent perspectives on landscape connectivity reveal consistent effects from genes to communities. Current Landscape Ecology Reports 1:67–79.

Fletcher, R. J., T. J. Hefley, E. P. Robertson, B. Zuckerberg, R. A. McCleery, and R. M. Dorazio. 2019. A practical guide for combining data to model species distributions. Ecology 100:e02710.

Forman, R. T. T. 2000. Estimate of the Area Affected Ecologically by the Road System in the United States. Conservation Biology 14:31–35.

GBIF.org. 2022. GBIF Occurrence Download https://doi.org/10.15468/dl.vg9kgm (accessed 20 May 2022). The Global Biodiversity Information Facility.

Gibson, L., E. N. Wilman, and W. F. Laurance. 2017. How green is 'green' energy? Trends in Ecology & Evolution 32:922–935.

Golding, N. 2019. greta: simple and scalable statistical modelling in R. Journal of Open Source Software 4:1601.

Gorelick, N., M. Hancher, M. Dixon, S. Ilyushchenko, D. Thau, and R. Moore. 2017. Google Earth Engine: Planetary-scale geospatial analysis for everyone. Remote Sensing of Environment 202:18–27.

Gray, M. E., B. G. Dickson, K. E. Nussear, T. C. Esque, and T. Chang. 2019. A range-wide model of contemporary, omnidirectional connectivity for the threatened Mojave desert tortoise. Ecosphere 10:e02847.

Grimmett, L., R. Whitsed, and A. Horta. 2020. Presence-only species distribution models are sensitive to sample prevalence: Evaluating models using spatial prediction stability and accuracy metrics. Ecological Modelling 431:109194.

Haddad, N. M., L. A. Brudvig, J. Clobert, K. F. Davies, A. Gonzalez, R. D. Holt, T. E. Lovejoy, J. O. Sexton, M. P. Austin, C. D. Collins, W. M. Cook, E. I. Damschen, R. M. Ewers, B. L. Foster, C. N. Jenkins, A. J. King, W. F. Laurance, D. J. Levey, C. R. Margules, B. A. Melbourne, A. O. Nicholls, J. L. Orrock, D.-X. Song, and J. R. Townshend. 2015. Habitat fragmentation and its lasting impact on Earth's ecosystems. Science Advances 1:e1500052.

Haight, R. G., B. Cypher, P. A. Kelly, S. Phillips, H. P. Possingham, K. Ralls, A. M. Starfield, P. J. White, and D. Williams. 2002. Optimizing Habitat Protection Using Demographic Models of Population Viability. Conservation Biology 16:1386–1397.

Hastie, T., R. Tibshirani, and J. Friedman. 2009. The Elements of Statistical Learning: Data Mining, Inference, and Prediction. Second edition. Springer, New York, NY.

He, K., X. Zhang, S. Ren, and J. Sun. 2016. Identity Mappings in Deep Residual Networks. Pages 630–645 *in* B. Leibe, J. Matas, N. Sebe, and M. Welling, editors. Computer Vision – ECCV 2016. Springer International Publishing, Cham.

Hobbs, N. T., and M. B. Hooten. 2015. Bayesian Models: A Statistical Primer for Ecologists. Princeton University Press.

Hollingsworth, B., P. Valcarcel, M. Rochell, K. Clark, and M. Stepek. 2017. Flat-tailed HornedLizard (Phrynosoma mcallii) (FTHL) Range-wide Habitat Model. Final Report, prepared for the Bureau of Land Management.

Howard, J., and S. Gugger. 2020. Fastai: A Layered API for Deep Learning. Information 11:108.

Hromada, S. J., T. C. Esque, A. G. Vandergast, K. E. Dutcher, C. I. Mitchell, M. E. Gray, T. Chang, B. G. Dickson, and K. E. Nussear. 2020. Using movement to inform conservation corridor design for Mojave desert tortoise. Movement Ecology 8:1–18.

Inman, R. D., T. C. Esque, K. E. Nussear, P. Leitner, M. D. Matocq, P. J. Weisberg, T. E. Dilts, and A. G. Vandergast. 2013. Is there room for all of us? Renewable energy and Xerospermophilus mohavensis. Endangered Species Research 20:1–18.

Iverson, A., D. P. Waetheb, and F. M. Shilling. 2021. Evidence-based wildlife connectivity assessment: Mojave Desert region. Road Ecology Center, University of California, Davis.

Johnston, A., W. M. Hochachka, M. E. Strimas-Mackey, V. R. Gutierrez, O. J. Robinson, E. T. Miller, T. Auer, S. T. Kelling, and D. Fink. 2021. Analytical guidelines to increase the value of community science data: An example using eBird data to estimate species distributions. Diversity and Distributions 27:1265–1277.

Jones, A. S., J. J. Anderson, B. G. Dickson, S. Boe, and E. S. Rubin. 2017. Off-highway vehicle road networks and kit fox space use. The Journal of Wildlife Management 81:230–237.

Landau, V. A., V. B. Shah, R. Anantharaman, and K. R. Hall. 2021. Omniscape.jl: Software to compute omnidirectional landscape connectivity. Journal of Open Source Software 6:2829.

Loft, E., D. Armentrout, G. Smith, D. Craig, M. Chapel, J. Willoughby, C. Roundtree, T. Mansfield, S. Mastrup, and F. Hall. 1998. An Assessment of Mule and Black-tailed Deer Habitats and Populations in California. Page 56. Report to the Fish and Game Commission, California Department of Fish and Wildlife, Sacramento CA.

Lovich, J. E., and J. R. Ennen. 2011. Wildlife conservation and solar energy development in the desert southwest, United States. BioScience 61:982–992.

Marine Corps. 2011. Final Biological Assessment: Land acquisition and airspace establishment to support large-scale marine air ground task force live-fire and maneuver training. Marine Corps Air Ground Combat Center, Twentynine Palms, CA.

Marshal, J. P., V. C. Bleich, P. R. Krausman, M. L. Reed, and N. G. Andrew. 2006. Factors Affecting Habitat Use and Distribution of Desert Mule Deer in an Arid Environment. Wildlife Society Bulletin 34:609–619.

McClure, M. L., B. G. Dickson, and K. L. Nicholson. 2017. Modeling connectivity to identify current and future anthropogenic barriers to movement of large carnivores: A case study in the American Southwest. Ecology and Evolution 7:3762–3772.

McClure, M., V. Landau, and B. G. Dickson. 2020. Tools for informing renewable energy project development to support recovery of the Mojave desert tortoise: Phase 2. Areas of Critical

Environmental Concern. Final Report, Conservation Science Partners, Inc., Truckee, CA.
McRae, B. H., B. G. Dickson, T. H. Keitt, and V. B. Shah. 2008. Using circuit theory to model connectivity in ecology, evolution, and conservation. Ecology 89:2712–2724.
McRae, B., K. Popper, A. Jones, M. Schindel, S. Buttrick, K. Hall, R. Unnasch, and J. Platt. 2016. Conserving nature's stage: Mapping omnidirectional connectivity for resilient terrestrial landscapes in the Pacific Northwest. The Nature Conservancy, Portland, OR.
Miguet, P., H. B. Jackson, N. D. Jackson, A. E. Martin, and L. Fahrig. 2016. What determines the spatial extent of landscape effects on species? Landscape Ecology 31:1177–1194.
Newman, M. E. J. 2005. A measure of betweenness centrality based on random walks. Social Networks 27:39–54.
Peaden, M. J., J. A. Nowakowski, T. D. Tuberville, K. A. Buhlmann, and B. D. Todd. 2017. Effects of roads and roadside fencing on movements, space use, and carapace temperatures of a threatened tortoise. Biological Conservation 214:13–22.
Pease, K. M., A. H. Freedman, J. P. Pollinger, J. E. Mccormack, W. Buermann, J. Rodzen, J. Banks, E. Meredith, V. C. Bleich, R. J. Schaefer, K. Jones, and R. K. Wayne. 2009. Landscape genetics of California mule deer (Odocoileus hemionus): the roles of ecological and historical factors in generating differentiation. Molecular Ecology 18:1848–1862.
Phillips, S. J., M. Dudík, J. Elith, C. H. Graham, A. Lehmann, J. Leathwick, and S. Ferrier. 2009. Sample selection bias and presence-only distribution models: implications for background and pseudo-absence data. Ecological Applications 19:181–197.
Pimm, S. L., and P. Raven. 2000. Extinction by numbers. Nature 403:843–845.
Poessel, S. A., P. Leitner, R. D. Inman, T. C. Esque, and T. E. Katzner. 2022. Demographic and environmental correlates of home ranges and long-distance movements of Mohave ground squirrels. Journal of Mammalogy:gyac082.
R Core Team. 2021. R: A language and environment for statistical computing. R Foundation for Statistical Computing, Vienna, Austria.
Rayfield, B., M.-J. Fortin, and A. Fall. 2011. Connectivity for conservation: a framework to classify network measures. Ecology 92:847–858.
Renner, I. W., J. Elith, A. Baddeley, W. Fithian, T. Hastie, S. J. Phillips, G. Popovic, and D. I. Warton. 2015. Point process models for presence-only analysis. Methods in Ecology and Evolution 6:366–379.
Shanley, C. S., and S. Pyare. 2011. Evaluating the road-effect zone on wildlife distribution in a rural landscape. Ecosphere 2:art16.
Shuford, and T. Gardali, editors. 2008. California Bird Species of Special Concern: A ranked assessment of species, subspecies, and distinct populations of birds of immediate conservation concern in California. Western Field Ornithologists & California Department of Fish and Wildlife, Sacramento CA.
Sullivan, B. L., C. L. Wood, M. J. Iliff, R. E. Bonney, D. Fink, and S. Kelling. 2009. eBird: A citizen-based bird observation network in the biological sciences. Biological Conservation 142:2282–2292.
Suraci, J. P., C. E. Littlefield, C. C. Nicholson, M. C. Hunter, A. Sorensen, and B. G. Dickson. 2022, October 10. Mapping connectivity and conservation opportunity on agricultural lands across the conterminous United States. bioRxiv Preprint. bioRxiv.
Suraci, J. P., B. A. Nickel, and C. C. Wilmers. 2020. Fine-scale movement decisions by a large carnivore

inform conservation planning in human-dominated landscapes. Landscape Ecology 35:1635–1649.

Takaku, J., T. Tadono, K. Tsutsui, and M. Ichikawa. 2016. Validation of “AW3D” global DSM generated from ALOS PRISM. ISPRS Annals of Photogrammetry, Remote Sensing & Spatial Information Sciences 3.

Theobald, D. M. 2013. A general model to quantify ecological integrity for landscape assessments and US application. Landscape Ecology 28:1859–1874.

Theobald, D. M., D. Harrison-Atlas, W. B. Monahan, and C. M. Albano. 2015. Ecologically-relevant maps of landforms and physiographic diversity for climate adaptation planning. PLOS ONE 10:e0143619.

Thornton, M. M., R. Shrestha, Y. Wei, P. E. Thornton, S.-C. Kao, and B. E. Wilson. 2020. Daymet: Daily Surface Weather Data on a 1-km Grid for North America, Version 4. ORNL DAAC.

U.S. Census Bureau. 2019. TIGER/LINE Shapefiles.

U.S. Geological Survey. 2022. USGS National Hydrography Dataset Best Resolution (NHD) for Hydrological Unit (HU) 4 (published 20220316). https://www.usgs.gov/national-hydrography/access-national-hydrography-products.

Wang, P., C. Huang, E. C. Brown de Colstoun, J. C. Tilton, and B. Tan. 2017. Global Human Built-up And Settlement Extent (HBASE) Dataset from Landsat. Palisades, NY: NASA Socioeconomic Data and Applications Center (SEDAC).

Zoellick, B. W., N. S. Smith, and R. S. Henry. 1989. Habitat use and movements of desert kit foxes in western Arizona. The Journal of Wildlife Management 53:955–961.

Zuur, A. F., E. N. Ieno, N. Walker, A. A. Saveliev, and G. M. Smith. 2009. Mixed effects models and extensions in ecology with R. Springer New York, New York, NY.

Appendix A - Habitat suitability models: Detailed methods and results

A1. Mule deer habitat suitability

Dataset preparation

Given the relatively harsh conditions of the Mojave and Sonoran deserts, mule deer (MD) either occur at low densities or are absent across much of the CDCA (Loft et al. 1998). However, several MD populations use portions of the CDCA and surrounding landscapes, including populations of Inyo mule deer in the north, Southern mule deer along the western edge, and burro deer in the southern and eastern portions of the CDCA (Loft et al. 1998, Pease et al. 2009). Our objective was to develop a species distribution model that describes general habitat suitability for all MD populations across the CDCA and surrounding areas. We therefore endeavored to obtain MD detection and location data from each of the populations that occupy our study area, focusing on a 50 km buffer around the CDCA to ensure that data represented the full range of habitats used by deer in this region (see Fig. A1.1). To that end, we acquired data from the following sources:

1. Helicopter surveys conducted by the California Department of Fish and Wildlife (CDFW) across the southern and eastern portion of the CDCA between 1991 and 2019 (59 detections)
2. MD occurrence records spanning the entire study area (833 total records) compiled by the Global Biodiversity Information Facility (GBIF) between 2003 and 2022 (GBIF.org 2022)
3. VHF collar data collected from 52 individual burro deer (4,013 total locations) from the Imperial County deer herd (southeastern corner of the study area) between 1999 and 2004 (Marshal et al. 2006)
4. VHF and GPS collar data collected by CDFW from 125 individual deer (20,372 total locations) in California's Peninsular Range (western border of the study area) between 2001 and 2007.

To standardize these data and minimize the influence of spatial bias, we spatiotemporally subsampled the combined dataset by overlaying a 5 km x 5 km square grid across the study area and randomly selecting at most a single deer point per year in each grid cell (i.e., more than one point could be retained within a single grid cell if those points were collected in different years). This approach helps to reduce the over-influence of well-surveyed areas (Johnston et al. 2021) while still allowing those areas that are regularly used by deer (i.e., where deer were detected in multiple years) to be well represented in the dataset. This process resulted in a final sample size of 859 deer locations (CDFW helicopter surveys, n = 42; GBIF, n = 401; Imperial VHF collar study, n = 250; Peninsular Range VHF and GPS collar study, n= 166). The Imperial and Peninsular Range collaring datasets in particular were substantially reduced by spatiotemporal subsampling (94% and 99% reductions, respectively), which we considered a necessary step to allow the integration of these highly structured collaring datasets with detection data collected either haphazardly (GBIF) or under temporally constrained conditions (irregular CDFW helicopter surveys). We acknowledge, however, that, while our spatiotemporal subsampling procedure addresses over-representation by some datasets and helps to deal with potential spatial bias stemming from, e.g., over-sampling of deer detection data near roads or in popular recreation areas, it cannot fully account for differences in how these datasets were collected and any potential biases introduced in the data by the sampling protocols used (Fletcher et al. 2019). However, in our view, the benefits of including

data from all deer populations in/near the CDCA outweighs the costs of using data collected under multiple sampling protocols when developing a habitat suitability model for the entire study area, and the capacity of our model to predict both in-sample and out-of-sample data (see below) suggests that unmodeled aspects of data collection had limited influence on model performance.

After subsampling, all deer points were considered to represent deer presence locations (rather than, e.g., points along a movement path) and were combined with random background locations to model habitat suitability. For GLM-based species distribution models (as used here, see below), performance has been shown to benefit from a relatively large ratio of background to presence locations (Grimmett et al. 2020). We therefore derived background locations (n = 7,677) by randomly selecting a single point in each cell of the 5 km x 5 km grid overlaid on the study area, leading to a ~ 9:1 background:presence ratio. Because the deer data used here were collected over a large time span (1991-2021), we binned each data point into one of six five-year bins (1990-1994, 1995-1999, etc, with the last bin encompassing 2015-2021) to facilitate associating each data point with climate or landscape covariate data representing a similar timeframe (see below). Background points were assigned the year of the nearest deer detection prior to binning.

Habitat suitability model covariates

All covariate data were summarized within a 1-km buffer around each deer presence and background location, allowing us to account for (1) potential spatial error in the exact location of each deer detection or relocation point, and (2) the fact that space use by large, mobile animals is often influenced by the broader habitat context rather than just the animal's immediate location (Miguet et al. 2016). Data layers describing several covariates of interest were available as time series and therefore provided an opportunity for temporal matching with MD location data. We acquired 30-m resolution, annual data (1990-2021) on percent cover of trees and shrubs and total aboveground herbaceous biomass from the Rangeland Analysis Platform (RAP; https://rangelands.app/) and, for each temporal bin (e.g. 1990-1994, 1995-1999, etc), calculated the mean value of each covariate (e.g., mean annual percent tree cover) for each pixel across the study area. We then took the average value within a 1-km buffer around each deer presence and background point. We acquired data on additional land cover types from the National Landcover Dataset (NLCD; Dewitz and U.S. Geological Survey 2021), which provides data at irregular intervals between 2001 and 2019. For each temporal bin, we selected a representative NLCD product: 2001 (1990-1994 and 1995-1999 temporal bins), 2004 (2000-2005 bin), 2008 (2005-2009 bin), 2013 (2010-2014 bin), or 2016 (2016-2021 bin). Each 30-m NLCD pixel is categorized as a single cover class. We acquired data on developed areas (NLCD classes 21 to 24), agriculture (NLCD classes 81 and 82), and water (NLCD class 11). Each covariate was summarized as the percent cover (i.e., percent of pixels categorized as the cover type of interest) within a 1-km buffer around each presence and background location. Finally, we acquired temporally variable data on two climate covariates that we hypothesized would be most relevant to predicting mule deer habitat suitability – mean daily maximum summer temperature (defined as maximum daily temperature from April through September) and mean daily precipitation. Climate variables were derived from Daymet V4 data (1-km resolution; Thornton et al. 2020). For each pixel across the study area, we calculated the average covariate value across all relevant days (i.e., only summer days for max temperature) within each deer temporal bin and then extracted the

mean value for the appropriate temporal bin within a 1-km buffer around each deer presence and background location.

Several covariates were considered to be static across the timespan of deer location data, either because of data limitations or because the covariate indeed does not vary over relevant timescales. We estimated several topographic variables, including elevation, slope, and aspect, derived from the ALOS DSM digital elevation model V3.2 (30-m resolution; Takaku et al. 2016) and the continuous heat insulation load index (CHILI, a measure of solar insolation) developed by Theobald et al. (2015). The mean value of each topographic variable was summarized within a 1-km buffer around each deer presence and background location. Finally we also calculated the percent cover of microphyll woodland within 1-km of each deer point, using the microphyll layer developed for the present analysis and described in Appendix B, Section B4. All covariate data were derived in Google Earth Engine (Gorelick et al. 2017) and exported at a common resolution of 90 m.

Model fitting, comparison, and validation

We randomly divided our data into training (80%) and test (20%) datasets and fit a suite of six candidate logistic regression models to the training dataset. Each candidate model represented a plausible hypothesis for the factors affecting deer habitat suitability and included a subset of the covariates described above, as well as quadratic terms for some covariates to capture potential non-linear effects. Each candidate model is described in Table A1.1. All logistic regression models were fit using the *glm* function in R (R Core Team 2021) with deer presence (1) or background (0) as the response variable, and the top model was identified based on AICc (Burnham and Anderson 2002).

To validate our top model, we quantified its ability to predict withheld test data based on the area under the receiver-operator characteristic curve (AUC; Hastie et al. 2009), which varies between 0 (no predictive ability) and 1 (perfect predictive ability). We also calculated the Boyce index (Boyce et al. 2002) which quantifies the correlation between habitat quality predicted by the model and the species locations. The Boyce index was calculated for both training data and test data. This index also varies between zero and one. Our validation metrics indicated very high predictive power of our top model, with an AUC score of 0.803 and Boyce Index scores of 0.953 (training data) and 0.607 (test data). Using our top model equation and, where applicable, the most recent temporally variable covariates (i.e., those corresponding to the 2015-2021 temporal bin), we then predicted mule deer habitat suitability (i.e., probability of occurrence) across the entire study area, consisting of the CDCA and 100km buffer (Fig. A1.1)

Table A1.1. Model selection results for mule deer logistic regression species distribution models.

Covariates	AUC	Deviance Explained	AIC	ΔAIC
Elevation + Elevation^2 + Slope + Slope^2 + Shrub + Shrub^2 + Tree + Tree^2 + HerbBiomass + Microphyll + Microphyll^2 + Development + Development ^{2} + Ag + Ag^2 + Water +SummerPrecip	0.803	0.219	3507.4	0.0
Elevation + Slope + CHILI + Microphyll + Shrub + Tree + Ag + SummerPrecip	0.786	0.15	3804.2	296.8
Elevation + Slope + CHILI + Aspect + Microphyll + Shrub + Tree + Ag + Development + SummerPrecip	0.786	0.15	3807.6	300.2
Shrub + Tree + HerbBiomass + Water +Water + Ag + Development + Microphyll + SummerPrecip	0.766	0.134	3875.2	367.8
Shrub + Tree + HerbBiomass + Microphyll + Water + Ag + Development	0.769	0.133	3877.9	370.5
Elevation + Slope + Aspect + CHILI	0.731	0.033	4318.0	810.6

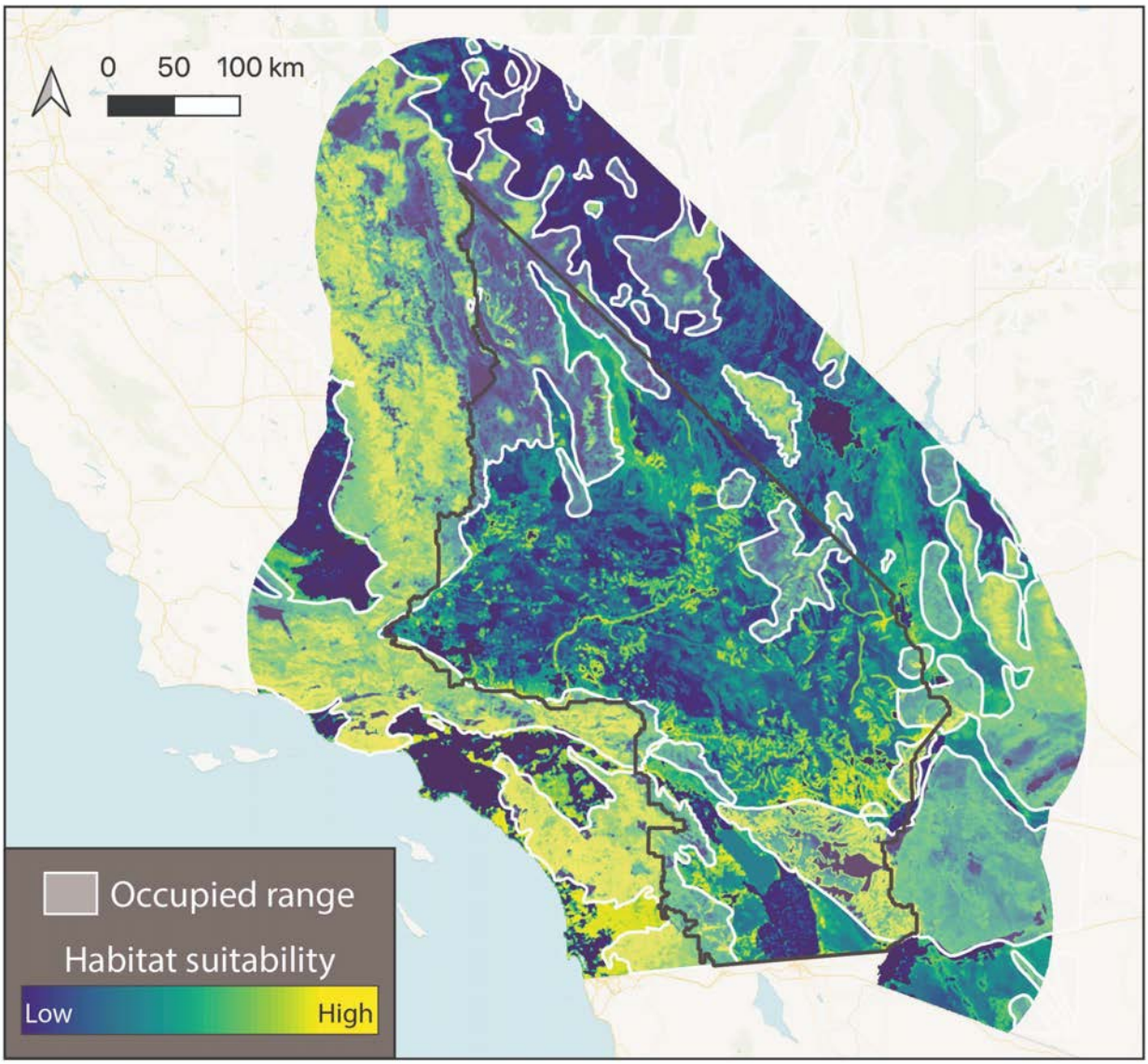

Figure A1.1. Mule deer habitat suitability, as predicted by the top linear regression-based species distribution model. Transparent white polygons denote expert-derived mule deer occupied range, as identified by the Western Association of Fish and Wildlife Agencies Mule Deer Habitat data layer (details here). Occupied range polygons were used to delineate potential deer movement start and endpoints in the MD source strength layer, as described in the main text.

A2. Desert kit fox habitat suitability

Data and covariate preparation

As noted in the main text, desert kit fox (DKF) models were developed using location data obtained from iNaturalist, a citizen science database of species observations (https://www.inaturalist.org/). We eliminated all observations with missing or unavailable coordinates, as well as those that fell outside of the study area. This resulted in a total of 123 DKF locations taken predominantly between 2004 and 2021 (with two observations from 1996).

Covariates for kit fox were chosen following guidance from the literature (Zoellick et al. 1989, Dempsey et al. 2015, Jones et al. 2017). Topographic covariates included the topographic position index (TPI), the topographic roughness index (roughness), slope, and the continuous heat insolation load index (CHILI, a measure of solar insolation, (Theobald et al. 2015)). Topographic variables were derived from the ALOS DSM digital elevation model V2.2 (Takaku et al. 2016). Climate variables included mean summer temperature (calculated as the mean daily temperature between April and September between 2010 and 2020; SummerTemp) and mean summer precipitation (calculated as the mean daily precipitation between April and September between 2010-2020; SummerPrecip). Climate variables were derived from Daymet V4 data (1-km resolution; Thornton et al. 2020). Finally, we included a set of land cover variables including percent shrub cover (Shrub), and percent built up/developed cover (Build) derived from the 2016 NLCD land cover product (Dewitz 2019) as well as pixel-wise median NDVI (calculated from the Landsat 5 and 8 imagery collections) between 2010 and 2020. All covariates were processed in Google Earth Engine, exported at 30-m resolution and centered and scaled prior to model fitting.

Model fitting

Prior to model fitting, we spatially subsampled the presence locations to reduce the influence of small areas with higher sampling effort and therefore more presence observations. To do so, we constructed a hexagonal grid using the *dgconstruct* function from the *dggridr* package in R with a spacing of 0.5 km (resulting in a grid spacing of 0.621km). For each hexagon in the mesh, we then randomly retained a maximum of one presence point. This resulted in a total of 105 presence locations for DKF. Subsampled points were then buffered by 30 km and the resulting polygons were dissolved to produce a single area for sampling random background locations. We randomly sampled 10 background locations for each presence location, ensuring that each background location was at least 1 km from the nearest presence location. Presence (1) and background (0) data were modeled as a function of environmental covariates using Bayesian logistic regression via the *greta* package in R (Golding 2019, R Core Team 2021). All models were fit using weakly informative priors, three chains, and 4,000 sampling iterations per chain with 500 burn-in iterations. We fit a set of 12 candidate models where each candidate model represented a plausible hypothesis for the factors affecting desert kit fox habitat suitability and included a subset of the covariates described above, as well as quadratic terms for some covariates to capture potential non-linear effects. Each candidate model is described in Table A2.1. The top model was identified by selecting the model with the minimum deviance information criterion (DIC), a generalization of the Akaike information criterion (AIC) that is often used in Bayesian model selection procedures (Hobbs and Hooten 2015). Wwe calculated the Boyce Index for our top model (i.e., the

model with the lowest DIC) using the full set of location data used to fit the model. The Boyce Index of our top model was 0.407.

Table A2.1. Model selection results for desert kit fox Bayesian logistic regression species distribution models.

Covariates	DIC	ΔDIC
Ag + Ag^2 + Build + $Build^2$ + NDVI + $NDVI^2$ + Shrub + $Shrub^2$ + Roughness + Slope + CHILI + SummerPrecip + SummerTemp + $SummerTemp^2$	671.7	0.0
Roughness + Slope + CHILI + SummerPrecip + SummerTemp + $SummerTemp^2$ + NDVI + $NDVI^2$ + Shrub + $Shrub^2$ + Ag + Build	677.1	5.4
Roughness + Slope + CHILI + SummerPrecip + SummerTemp + $SummerTemp^2$ + NDVI + $NDVI^2$ + Shrub + $Shrub^2$	678.7	7.0
Roughness + Slope + CHILI + SummerPrecip + SummerTemp + NDVI + Shrub	680.6	8.9
Roughness + Slope + CHILI + NDVI + $NDVI^2$ + Shrub + $Shrub^2$	682.3	10.6
SummerPrecip + SummerTemp + Summer $Temp^2$	682.7	10.9
SummerPrecip + SummerTemp	683.6	11.9
Roughness + Slope + CHILI + SummerPrecip + SummerTemp + Summer $Temp^2$	683.6	11.9
Roughness + Slope + CHILI + SummerPrecip + SummerTemp	684.5	12.8
Roughness + Slope + CHILI + NDVI + Shrub	684.6	12.9
Roughness + Slope + CHILI	695.7	24.0

Appendix B - Major updates to resistance surface inputs

B1. Roads, railways, and crossing structures

Road resistance

An overall objective of this work was to develop models that reflect the substantial difficulty experienced by wildlife in the California desert region in crossing major roads and thereby identify movement pathways and corridors that either avoid major roads or reflect existing locations of lower road resistance (e.g., potential crossing structures such as bridges and culverts). Building on methods developed in the Phase I analysis, we therefore treated roads as exerting very high resistance to movement. Line data on roads were derived from the TIGER roads database (U.S. Census Bureau 2019). The effects of a road occur beyond the physical road itself, potentially impacting wildlife movement in a zone extending out from the road edge (Forman 2000, Shanley and Pyare 2011). To better reflect the barriers presented by primary and secondary roads and overpasses (TIGER MTFCC codes 1100, 1200, and 1630), we buffered each of these features by a set width corresponding to approximately 180 m in our final resistance rasters. We also included local roads (MTFCC code S1400) in all resistance surfaces, which were assigned as smaller width (approx. 90 m) in final resistance rasters, reflecting the small size and impact of these roads.

The resistance values associated with each road type depended on the focal species considered. As noted in the main text, we defined species- and road type-specific resistance factors, which were then multiplied by R_{max} (i.e., maximum resistance value associated with human land use intensity) and added to the final resistance surface. For reptile species with relatively low mobility (MDT and FTHL), primary roads were treated as complete barriers (i.e., impossible for current to flow across), as advised by project partners in the U.S. Fish and Wildlife Service (USFWS). Secondary and local roads were assigned resistance multipliers of 5 and 1, respectively (i.e., secondary roads were considered to be up to 5 times as resistant as other heavily developed landscapes). For mammal species, the barrier effects of roads are known to decrease with increasing body size (Chen and Koprowski 2019). We therefore assigned the largest resistance multipliers for the smallest mammal species, MGS (20, 5, and 1 for primary, secondary, and local, respectively), and assigned decreasing multipliers of increasingly large bodied species (DKF: 12, 3, 0.8; DBS and MD: 8, 2, 0.5). For the only bird species considered here (LCTH), we assumed that roads would be no more resistant than other heavily developed areas (given the species' ability to fly over roads) and assigned all road types a resistance multiplier of 1. Primary overpasses were assigned the same resistance multiplier as primary roads. We note that, while these road resistance multipliers are somewhat arbitrary, they achieve the desired goal of generating high road resistance, as compared to other landscape features, while taking advantage of the fact that relative differences in resistance values (e.g., relative difference between primary and secondary roads) are the most relevant factor in determining the ultimate connectivity surface.

For all species, we set all road pixels to zero in our source strength layers to ensure that current could not originate from these locations on the landscape. For MDT, we additionally took advantage of findings

from Peaden et al. (2017) as well as GIS data on tortoise highway fencing (provided by USFWS collaborators) to define broader areas around primary and secondary roads where source strength was also set to zero. Tortoise mortality is known to increase in areas around highways where tortoise fencing does not exist. We therefore created "road exclusion zones" along highways with no fencing by buffering the primary and secondary road features to reflect the exclusion zone distances estimated by Peaden et al.'s breakpoint analysis. Primary roads were buffered to a distance of 306m and secondary roads were buffered to a distance of 230m, with buffered areas set to zero source strength.

Railway resistance

We incorporated railway features using data from the North American Rail Lines National Geospatial Data Asset (Federal Railroad Administration 2016). As with primary and secondary roads, railway line features were buffered by a set amount resulting in an approximate width of 180 m in the final resistance rasters. Relatively little literature exists that empirically evaluates the effect of railways on the movement of the focal species. For DKF, MD, DBS, and MGS, we therefore assumed that railway lines exert the same resistance as secondary roads (see above). For LCTH, we assumed that rail lines exert no additional resistance to movement based on the ability of birds to fly over them. A telemetry study performed by Hromada et al. (2020) suggested that railways, in combination with the construction of flood mitigation berms surrounding the tracks themselves, pose significant barriers to Mojave desert tortoise given their mobility constraints. Given this strong potential barrier effect, we updated the MDT resistance surface generated by Gray et al. (2019) such that rail features were assigned the maximum resistance value possible. For FTHL, we assigned railways a resistance multiplier of 20, reflecting potentially similar constraints on movement imposed by the combination of the physical railway structures and rail traffic. Railways were set to zero source strength for all species.

Modifying resistance layers with potential crossing structures

As a major update for the Phase II analysis, we incorporated potential crossing structures (bridges and culverts) along primary and secondary highways to reduce the resistance imposed by linear road and railway features in the vicinity of these structures. To identify potential road crossings, we first downloaded the National Bridge Inventory (NBI) dataset (https://www.fhwa.dot.gov/bridge/snbi.cfm), as well as a California-specific bridge dataset maintained by CalTrans (https://caltrans-gis.dot.ca.gov/arcgis/rest/services/CHhighway/State_Highway_Bridges/FeatureServer/0). Point data from each dataset includes bridges over desert washes, rivers, and streams, as well as large box culverts (hereafter, referred to collectively as crossing structures). These datasets also include highway overpasses, but these were filtered out prior to further analysis. We evaluated the spatial overlap between the NBI and CalTrans datasets and merged structures that were labeled with the same identifier. We then buffered all crossing structure points to a distance of 200m and merged their geometries to better capture potential crossing opportunities that span highway medians or multi-lane highways. To approximate the size of the structures, we used the 'Length' field provided in the NBI and CalTrans datasets. This data field represents the total length of roadway that is supported on the structure, and therefore corresponds to the width of the crossing structure, as experienced by an animal crossing through. For each merged geometry feature outlined above, we assigned a 'width' attribute based on this length-of-road field. When more than one buffered crossing structure polygon was merged

(e.g., because the same structure was represented in both NBI and CalTrans datasets) we assigned the final polygon the minimum width value. We rasterized this final polygon layer at 90-m resolution, assigning pixel values based on width.

We used an empirical dataset on wildlife use of road crossing structures assembled by Denneboom et al. (2021) to estimate the degree to which crossing structures would reduce the resistance imposed by roads for each of our focal species. This dataset consists of published empirical estimates of the efficacy of wildlife crossing structures measured as the percent of successful crossings by animal taxonomic groups (i.e., amphibians and reptiles, small non-carnivores, ungulates, small carnivores, large carnivores) as a function of crossing structure width (among other factors). Using quantiles of the empirical distribution of crossing structure widths for each relevant taxonomic group in the Denneboom et al. dataset, we defined multiple structure width binds as follows: amphibians and reptiles, two width bins (≤ 3m wide, >3m wide); small non-carnivores, three width bins (≤ 3m, 3-10m, >10m), small carnivores and ungulates, three width bins (≤ 5m, 5-15m, >15m). For each taxonomic group, we then calculated the mean proportion of successful crossings (i.e., crossing probability) for structures within each width bin (Table B1.1). These crossing probability values were then used as multipliers to reduce the resistance of roads at crossing structure locations based on the width attribute of the structure. For example, the mean crossing success by small carnivores from the Denneboom et al. dataset for crossing structures ≤ 5m wide was 36%, so road resistance in the DKF resistance surface was multiplied by 0.36 in the vicinity of any crossing structures ≤ 5 m wide, thereby allowing more current to flow through the crossing structure than over the road itself.

Table B1.1. Crossing structure width bins and associated crossing probabilities (mean proportion of successful crossings) for each relevant taxonomic group from Denneboom et al. (2021)

Taxonomic group	Width bin	Crossing probability
Reptiles (MDT, FTHL)	≤ 3 m	0.35
	> 3 m	0.15
Small non-carnivore (MGS)	≤ 3 m	0.27
	3 to 10 m	0.50
	> 10 m	0.39
Small carnivore (DKF)	≤ 5 m	0.36
	5 to 15 m	0.43
	> 15 m	0.18
Ungulate (DBS, MD)	≤ 5 m	0.53
	5 to 15 m	0.45
	> 15 m	0.29

For railways, we acquired the Railroad Bridge dataset from the Homeland Infrastructure Foundation-Level Data (HIFLD) database (https://hifld-geoplatform.opendata.arcgis.com/), which represents all points where railways cross over a depression or an obstruction. Railway bridge points were buffered by a radius of 200 m, and converted to a raster at 90-m resolution. Unfortunately no information was available regarding the width of railway bridges, thus railway bridges were assigned a uniform resistance reduction equal to that of the largest width bin for each species.

Importantly, across both crossing structure datasets, there was no consistent information describing the vertical clearance of crossing structures, which is likely to be an important limiting factor affecting the probability of an animal using the structure. Thus our focus on crossing structure width in determining resistance reductions provides a plausible hypothesis for the effects of crossing structures on animal movement but may not capture all factors affecting crossing probability. Additionally, spatial uncertainty in the coordinates of crossing structures led in some cases to a small degree of misalignment between roads and structures. As such, the location of crossing structures should be considered approximate.

B2. OHV route density in open areas

Off-highway vehicle (OHV) use is prevalent throughout the California desert region and poses potential threats to many wildlife species. In addition to defined OHV trails across the region, for which at least partial data coverage exists (see description of Owlshead and WEMO OHV route data in the main text), OHV activity also occurs in "open areas" on BLM land. OHV activity is essentially permitted anywhere within the boundaries of open areas, though in practice, activity is likely to be concentrated within certain sections of a given open area due to, e.g., terrain constraints. However, to our knowledge, no information exists on variation in the intensity of OHV use within open areas. To improve our ability to estimate the impacts of OHV activity on wildlife movement, we trained a computer vision model to detect differences in OHV route density inside open areas using aerial imagery.

We acquired high resolution (0.6 m x 0.6 m) aerial imagery circa 2020 from the USDA's National Agriculture Imagery Program (NAIP; https://naip-usdaonline.hub.arcgis.com/). We randomly sampled NAIP imagery from across the CDCA by first generating 2,075 random points within the CDCA boundary and then extracting NAIP imagery "chips" (256 x 256 pixels or 153.6m x 153.6m) centered on each random point. Two trained observers scored each image chip as falling into one of four categories based on the number of OHV routes visible in the image (Fig. B2.1): no routes, one route, two-to-three routes, or four or more routes.

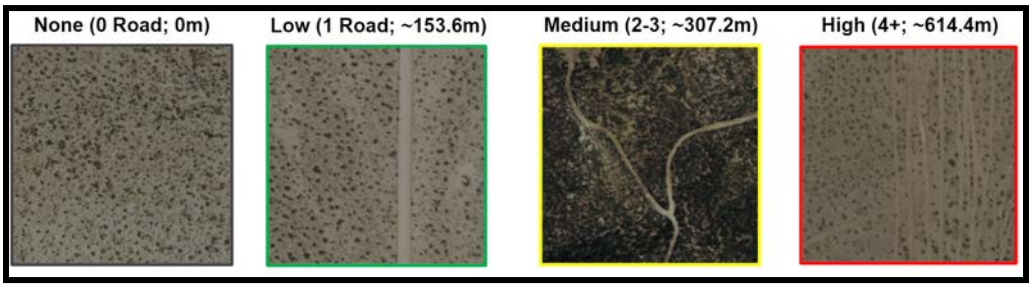

Figure B2.1. Example NAIP image chips falling into each of the four OHV route density categories

The scored NAIP chips were divided into training (n = 1,732) and test (n = 343) sets, and the training set was used to develop a computer vision (CV) model. The model used a residual network (Resnet101) architecture (He et al. 2016) and was built in FastAI (Howard and Gugger 2020). We validated the CV model by using it to predict OHV route density for the withheld test set and observed a model accuracy of 85% (290 correct of 343 images). We then predicted the CV model across all open areas in the CDCA using the open area polygons defined by the Desert Renewable Energy Conservation Plan (DRECP; see DRECP Base Plan dataset on DataBasin; https://drecp.databasin.org/). Finally, we smoothed the predicted OHV density layer using a gaussian kernel with 540-m radius to reduce the influence of small artifacts in the prediction surface. The resulting OHV density raster consisted of the four route density categories described above, coded from 0 (no OHV routes) to 3 (four or more routes) (Fig. B2.2). This layer was used as described in the main text to modify the resistance associated with locations inside of open areas, with the exact modifier depending on the scenario used.

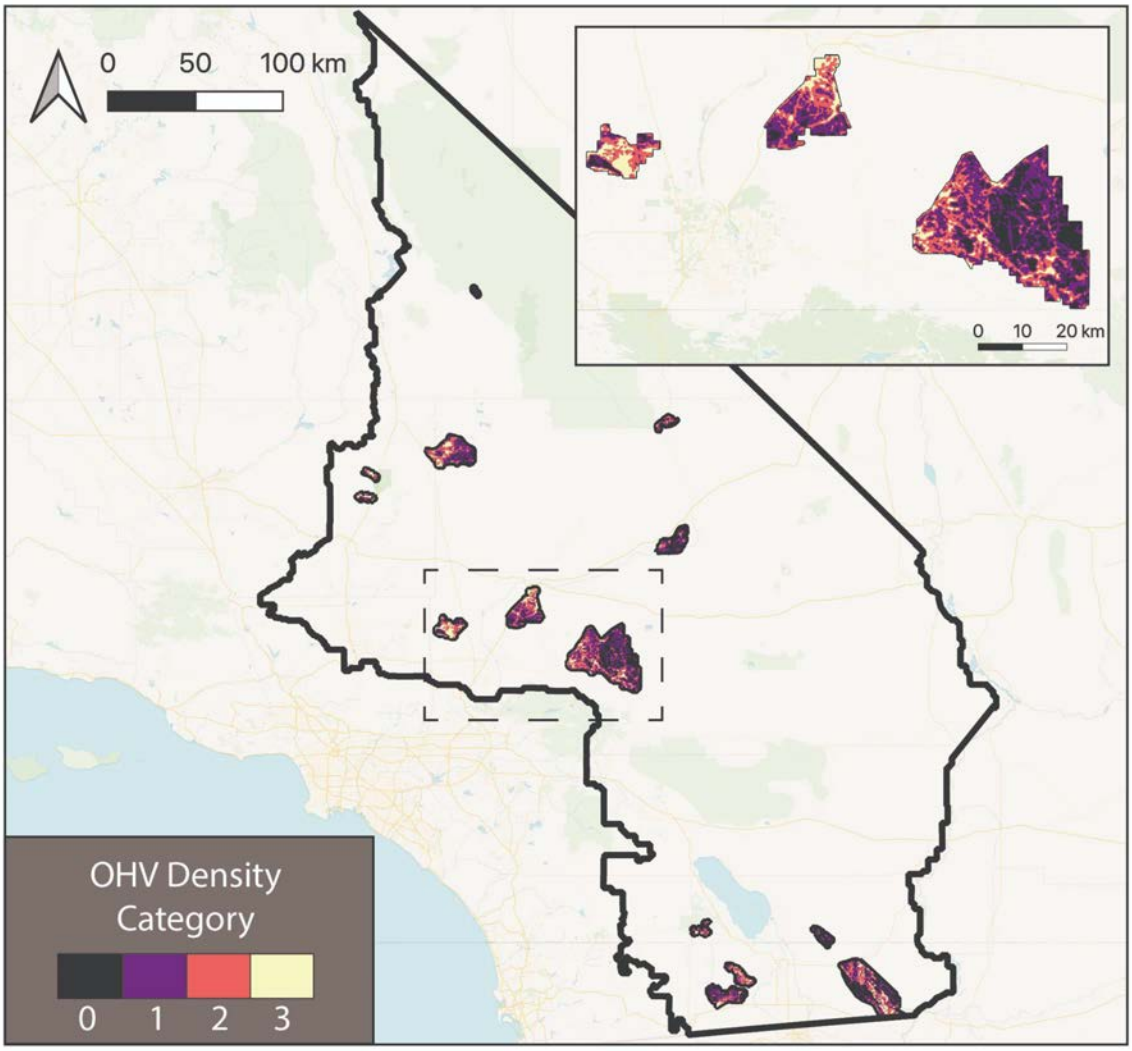

Figure B2.2. OHV route density within open areas, as predicted by the computer vision model. OHV route density was categorized into four levels: 0 (no routes), 1 (one route), 2 (two-to-three routes), 3 (four or more routes)

B3. Department of Defense lands

Several Department of Defense (DoD) installations occur within the CDCA, and military maneuvers on these installations may impact wildlife movement. In Phase I of this analysis, we applied a set resistance modifier to all pixels within the borders of all DoD installations, essentially treating the entire footprint of each installation as equally difficult to traverse. In this updated analysis, our aim was to base the resistance modifier associated with DoD lands on the estimated intensity of military activity, which varies within an installation. For this work, we focused on Fort Irwin and the Marine Corp Air Ground Combat Center at Twentynine Palms (MCAGCC), the two most intensively used military bases in the CDCA. In the absence of detailed spatial information on military maneuvers (e.g., weapons training/testing, motorized vehicle use) within each of these installations, we based our resistance modifiers on two factors: (1) "off-limits" areas, i.e., areas where maneuvers are restricted, which were considered to add no additional resistance beyond that determined by the underlying landscape (including any existing roads or other development), and (2) slope of the terrain, considered a proxy for intensity of activity (particularly vehicle use, see below).

We obtained spatial data on off-limits areas either directly from contacts within DoD (Fort Irwin) or from maps in publicly available reports (MCAGCC; Marine Corps 2011). For MCAGCC, a subset of areas that are currently off limits are anticipated to be open to maneuvers in the near future. We therefore created two off-limits areas datasets describing the present day and anticipated future footprints of off-limits areas across the two installations, with all off-limits areas assigned a resistance modifier of zero. A continuous slope raster was derived from the ALOS DSM digital elevation model V3.2 (30-m resolution; Takaku et al. 2016) and divided into five slope classes. Each slope class received a different resistance modifier value under the assumption that maneuver activity is likely to be greatest on flat ground and decrease with increasing slope, and that, beyond a certain slope, activity is restricted to low-impact, non-motorized uses. At MCAGCC, slopes above 22° are considered too steep for motorized vehicle use (Marine Corps 2011) and we therefore treated slopes at or above this level at both installations as having no additional anthropogenic resistance beyond that described by the underlying landscape (resistance modifier = 0). For all slopes less than 22°, we assigned resistance modifiers that decreased with increasing slope based on the following four categories: 0° to 4.9° (modifier = 0.5), 5° to 9.9° (0.375), 10° to 14.9° (0.25), and 15° to 21.9° (0.125). While these categories are somewhat arbitrary (by necessity, given the lack of spatial data on variation in actual maneuver intensity), they provide a reasonable set of assumptions regarding within-base differences in likelihood of intensive maneuvers. However, we acknowledge that slope is of course an imperfect proxy for all military activities (e.g., aerial weapons training) and is likely to predominantly capture maneuvers involving motorized vehicles. We developed two DoD resistance modifier layers based on the above, one describing present day maneuver intensity (i.e., incorporating existing off-limits areas) and one describing anticipated future maneuver intensity (i.e., incorporating anticipated future off-limits areas).

B4. Microphyll woodlands

Microphyll woodlands (MW) are a key vegetation community type in the California desert region, providing important habitat for a number of wildlife species (e.g., mule deer; Marshal et al. 2006). The DRECP Base Plan provides vector data on MW in the southern portion of the CDCA based on California

GAP analysis vegetation maps (https://drecp.databasin.org/). However, some users have noted that the DRECP MW polygons are overly restrictive in both spatial extent and in the range of plant species considered to constitute MW. In an effort to develop a more comprehensive data layer describing the approximate spatial footprint of MW in the CDCA, we combined the existing DRECP MW polygons with additional plant community distribution data from the California Department of Fish and Wildlife's 2016 Vegetation Classification and Mapping Program (VegCAMP) dataset (https://wildlife.ca.gov/Data/VegCAMP) and data on terrain features likely to support MW from the National Hydrography Dataset, Hydrologic Unit 4 (NHD; U.S. Geological Survey 2022). VegCAMP uses the National Vegetation Classification Standards (NVCS) to classify plant communities.

Based on consultation with BLM colleagues and other interested parties, we identified two NVCS groups in the VegCAMP dataset that were not included in the DRECP MW layer but contain plant species that are often associated with microphyll communities: (1) "Mojavean semi-desert wash scrub" and (2) "Sonoran-Coloradan semi-desert wash woodland/scrub". We extracted VegCAMP polygons labeled as one of these two NVCS groups. From the NHD, we extracted all polygons within the CDCA coded as "wash" (F Code 48400), which in this region captures desert washes or seasonal watercourses where MW communities often occur. We then unioned all three sets of polygons (DRECP MW, the two NVCS groups from VegCAMP, and desert washes from NHD) into a single vector dataset describing the spatial footprint of MW. Note that this dataset adopts a relatively permissive definition of MW (e.g., not all desert washes may contain MW communities). However, for the purposes of this work, including identifying suitable habitat for mule deer and incorporating MW into solar development projections, this comprehensive approach was considered appropriate. For the purposes of excluding sensitive habitat from solar development areas, we incorporated a legally mandated 200 ft "setback" area around MW by buffering our final layer by 200 ft (61 m).